

---

# Provable Ordering and Continuity in Vision-Language Pretraining for Generalizable Embodied Agents

---

Zhizhen Zhang<sup>1</sup> Lei Zhu<sup>2</sup> Zhen Fang<sup>3</sup> Zi Huang<sup>1</sup> Yadan Luo<sup>1</sup>

## Abstract

Pre-training vision-language representations on human action videos has emerged as a promising approach to reduce reliance on large-scale expert demonstrations for training embodied agents. However, prior methods often employ time contrastive learning based on goal-reaching heuristics, progressively aligning language instructions from the initial to the final frame. This overemphasis on future frames can result in *erroneous* vision-language associations, as actions may terminate early or include irrelevant moments in the end. To address this issue, we propose Action Temporal Coherence Learning (AcTOL) to learn *ordered* and *continuous* vision-language representations without rigid goal-based constraint. AcTOL treats a video as a continuous trajectory where it (1) contrasts semantic differences between frames to reflect their natural ordering, and (2) imposes a local Brownian bridge constraint to ensure smooth transitions across intermediate frames. Extensive imitation learning experiments across varying numbers of demonstrations show that the pretrained features significantly enhance downstream manipulation tasks by up to 49% with high robustness to different linguistic styles of instructions, offering a viable pathway toward generalized embodied agents. Our code is available [here](#).

## 1. Introduction

The long-term vision for embodied intelligence (Mu et al., 2023; Liu et al., 2024) is to create systems that seamlessly perceive and interact with the world around them. Achieving this requires agents that integrate vision and language to understand their surroundings, interpret human instructions, and autonomously plan actions for complex tasks. Current end-to-end approaches achieve policy learning through di-

rect vision-language-action mapping (Zitkovich et al., 2023; Cheang et al., 2024; Kim et al., 2024). However, the inherent unpredictability of physical environments, including unseen scenarios and dynamic object interactions, constrains these solutions by requiring massive, high-quality robotic trajectories with action annotations, which are *costly* to collect. To mitigate this, recent research has leveraged large-scale, readily available egocentric human action videos (Goyal et al., 2017; Damen et al., 2018; Grauman et al., 2022) for *pre-training*. Although these out-of-domain videos often lack low-level action details and contain noise, their diverse human-object interactions and task instructions provide valuable prior knowledge. This enables the pre-trained representations to be more effectively transferred to novel tasks with fewer demonstrations, reducing reliance on large-scale robotic datasets while preserving strong generalization capabilities.

A promising approach for vision-language pre-training from human action videos leverages the concept of *time contrastive learning* (Sermanet et al., 2018) to capture temporally consistent visual representations. In this framework, language serves as the guiding goal, with semantic alignment between the language and chronologically later frames in the video (Nair et al., 2022; Ma et al., 2023a; Li et al., 2024). However, this semantic alignment approach relies on a rigid assumption that action videos adhere to a specific principle: *actions progressively approach the target instruction from the initial frame to the final one*. Such assumption can be easily violated in real-world human action videos, which are typically annotated at a coarse-grained level and riddled with noise. The start and end points of actions are often ambiguous, and the progression may not consistently move toward the goal but instead exhibit fluctuations and detours. As a result, these methods struggle with misleading semantic alignment, leading to inaccurate vision-language relationships.

Given the challenges outlined above, a more natural and flexible pre-training strategy without rigid assumptions is needed to enhance vision-language representations for better policy learning. Building solely on the intrinsic temporal consistency of human action videos, we argue that the *ordering* and *continuity* of pre-trained vision-language

<sup>1</sup>The University of Queensland <sup>2</sup>Tongji University <sup>3</sup>University of Technology Sydney. Correspondence to: Yadan Luo <y.luo@uq.edu.au>.

representations play a crucial role in ensuring the effectiveness of policy learning. Ordering refers to the need for visual features to align with the underlying action logic required by the language instruction. For instance, as the task progresses, visual representations closer to the completion of the action should exhibit stronger alignment with the language instruction. This ensures that each step in the sequence is meaningfully associated with the corresponding instruction, enabling the model to effectively capture the dynamic progression of the task. Continuity, on the other hand, emphasizes that both visual features and their alignment with the language should evolve smoothly over time, with gradual transitions rather than abrupt changes. This is crucial because actions in the real world are not discrete but unfold continuously in time. Moreover, the alignment between visual and instruction should also be fluid, ensuring that as the action progresses, the visual representations consistently align with the target language instruction.

To address the aforementioned issues, we propose Action Temporal Coherence Learning (AcTOL), a novel approach designed to implicitly capture the ordering and continuity of video actions without relying on rigid assumptions, while providing strong theoretical guarantees. Unlike previous approaches that focus on goal-directed semantic alignment, AcTOL introduces a Vision-Language Ordering (VLO) loss. This loss leverages the intrinsic temporal coherence of videos, contrasting frames against each other based on their relative temporal distance, theoretically ensuring that the semantic alignment between frames reflects their temporal ordering and continuity throughout the entire sequence. However, the VLO loss does not explicitly enforce the continuity of the visual features themselves, and under conditions with variations in frame content and noise, it can lead to suboptimal local consistency of the visual features. To address this, AcTOL introduces a Brownian bridge constraint over the video, treating video frames as a Brownian bridge process. This approach imposes a structured, continuous flow on the visual representations, ensuring that the model learns more consistent and stable intermediate states, further enhancing the continuity of the visual representations and improving the stability of their alignment with language instruction. Further theoretical analysis suggests that these properties also contribute to the model’s resilience to language perturbations, a crucial trait for real-world applications. To validate the generalization ability of AcTOL on embodied agents, we conducted extensive language-conditioned imitation learning experiments in two simulation environments. The results show that AcTOL outperforms previous methods up to 49.0% with 5 (limited number of) expert demonstrations. Additionally, we performed an analysis of language-conditioned visual rewards on several real-world action videos. The findings reveal that the ordering and continuity of AcTOL enable it to serve as

a promising reward function, generating dense rewards that align well with the given instructions.

## 2. Related Work

Given the success of large-scale pre-training in the vision and language research communities (Brown et al., 2020; Liu et al., 2023), many studies have attempted to extend this paradigm to the field of robotics. Some work leverage massive robotic trajectory data (Collaboration et al., 2023) for pre-training, aiming to establish a unified mapping from the perception space to the action space (Zitkovich et al., 2023; Cheang et al., 2024). However, collecting large amounts of high-quality robot trajectory data is extremely costly and time-consuming. Consequently, many studies have begun to explore the use of large-scale, readily available, out-of-domain human action video data to learn generalizable representations that can be transferred to robotic tasks (Sermanet et al., 2018; Ma et al., 2023b; Radosavovic et al., 2022; Nair et al., 2022; Karamcheti et al., 2023; Ma et al., 2023a; Majumdar et al., 2023; Ye et al., 2024; Zeng et al., 2024; Li et al., 2024). Among these, TCN (Sermanet et al., 2018), VIP (Ma et al., 2023b), MVP (Radosavovic et al., 2022), and VC-1 (Majumdar et al., 2023) focus solely on studying unimodal visual representations, limiting their performance when understanding language instructions is required. R3M (Nair et al., 2022) employs language and reward models to shape progressive visual representations, while Voltron (Karamcheti et al., 2023) and MPI (Zeng et al., 2024) model the transition from the current state to the goal state conditioned on language. However, during training, these approaches freeze the language encoder, using it only to aid in the training of visual representations. As a result, they do not effectively achieve multi-modal representation learning.

Recently, LIV (Ma et al., 2023a) and DecisionNCE (Li et al., 2024) have attempted to leverage CLIP (Radford et al., 2021), a state-of-the-art vision-language model, to train embodied multi-modal representations. LIV treats language instructions as the goals of video actions and aligns the final frame of a video with the corresponding language description. DecisionNCE, on the other hand, views language as the transition from the initial state to the final state, aligning the difference between the representations of the first and last frames with the language. Their methods rely on goal-directed semantic alignment, which tends to produce suboptimal results under the noise present in real-world videos. In contrast, our approach avoids rigid assumptions, theoretically ensuring that semantic alignment follows the intrinsic temporal continuity and ordering of the video, resulting in more robust and generalizable vision-language representations.

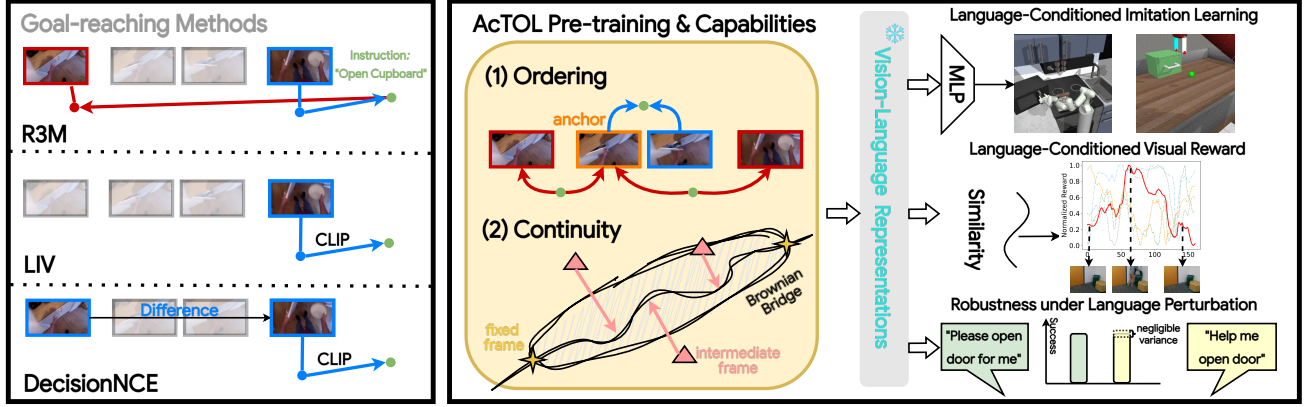


Figure 1. Comparison of existing *goal-reaching* pre-training strategies and the proposed AcTOL approach. The learned multi-modal representations can be effectively transferred to downstream language-conditioned robot manipulation tasks, exhibiting robustness to diverse instruction and linguistic variations.

Table 1. Comparison of different component designs in time contrast learning across mainstream vision-language pre-training.

| Method      | $\mathcal{P}(\mathcal{O}_i)$           | $\mathcal{N}(\mathcal{O}_i)$     | $\mathfrak{R}(\mathbf{v}, \mathbf{l}_i)$                                     |
|-------------|--|----------------------------------|--|
| R3M         | $(o_0, o_{j>i})$                       | $(o_0, o_i, o_j^{\#O_i})$        | reward $(\mathbf{v}, \mathbf{l}_i)$  |
| LIV         | $(o_T)$                                | $(o_T^{\#O_i})$                  | $\cos(\mathbf{v}, \mathbf{l}_i)$   |
| DecisionNCE | $(o_i, o_{j>i})$                       | $(o_i^{\#O_i}, o_j^{\#O_i})$     | $\cos(\mathbf{v}_j - \mathbf{v}_i, \mathbf{l}_i)$                            |
| AcTOL       | $(o_i, o_{j \in [T] \setminus \{i\}})$ | $(o_i, o_k : d_{i,k} > d_{i,j})$ | $-\ \cos(\mathbf{v}_i, \mathbf{l}_i) - \cos(\mathbf{v}_j, \mathbf{l}_i)\ _2$ |

### 3. Preliminaries

We first set up notations and mathematically formulate tasks.

**Language-Conditioned Imitation Learning (LC-IL).** The task of LC-IL aims to train an agent to mimic expert behaviors from a given demonstration set  $\mathcal{D}_d = \{(\tau_i, l_i)\}_{i=1}^N$ , where  $l_i \in \mathcal{L}$  represents a task-specific language instruction. Each trajectory  $\tau_i \in \mathcal{T}$  consists of a sequence of state-action pairs  $\tau_i = \{(s_j, \mathbf{a}_j)\}_{j=1}^T$  of the horizon length  $T$ . In robot manipulation tasks, action  $\mathbf{a}_j \in \mathcal{A}$  corresponds to the control commands executed by the agent and state  $\mathbf{s}_j = [\mathbf{p}_j; \mathbf{v}_j] \in \mathcal{S}$  records proprioceptive data  $\mathbf{p}_j$  (e.g., joint positions, velocities) and visual inputs  $\mathbf{o}_j \in \mathcal{O}$  (e.g., camera images) at the time step  $j$ . The objective of LC-IL is to find an optimal language-conditioned policy  $\pi^*(\mathbf{a}|s, l) : \mathcal{S} \times \mathcal{L} \mapsto \mathcal{A}$  via solving the supervised optimization as follows,

$$\pi^* \in \arg \min_{\pi} \mathbb{E}_{(\tau_i, l_i) \sim \mathcal{T}} \left[ \frac{1}{T} \sum_{(s_j, \mathbf{a}_j) \sim \tau_i} \ell(\pi(\hat{\mathbf{a}}_j, \mathbf{s}_j | l_i), \mathbf{a}_j) \right],$$

where  $\ell(\cdot, \cdot)$  is a task-specific loss, such as mean squared error or cross-entropy. Training the policy  $\pi_{\theta}$  in an end-to-end fashion may require *hundreds* of high-quality expert demonstrations to converge, primarily due to the high variance of visual inputs  $\mathbf{o}$  and language instructions  $l$ .

**Vision-language Pre-training.** Address such scalability issues can be achieved by leveraging large-scale, easily ac-

cessible human action video datasets  $\mathcal{D}_p = \{(\mathcal{O}_i, l_i)\}_{i=1}^M$  (Damen et al., 2018; Grauman et al., 2022), where  $\mathcal{O}_i = \{o_j\}_{j=1}^T$  represents a video clip with  $T$  frames and  $l_i$  the corresponding description. Pretraining on such datasets enables policies to rapidly learn visual-language correspondences with minimal expert demonstrations. Mainstream pretraining methods employ time contrastive learning (Sermanet et al., 2018) to fine-tune a visual encoder  $\phi$  and a text encoder  $\varphi$ , which project frames and descriptions into a shared  $d$ -dimensional embedding space, i.e.,  $\mathbf{v}_j = \phi(o_j) \in \mathbb{R}^d$  and  $\mathbf{l}_i = \varphi(l_i) \in \mathbb{R}^d$ . To provide a unified perspective on various pretraining approaches, we formulate them within the objective  $\mathcal{L}_{\text{tNCE}}(\phi, \varphi)$ :

$$\mathcal{L}_{\text{tNCE}} = -\mathbb{E}_{o^+ \sim \mathcal{P}(\mathcal{O}_i)} \log \frac{\exp(\mathfrak{R}(\mathbf{v}^+, \mathbf{l}_i))}{\mathbb{E}_{o^- \sim \mathcal{N}(\mathcal{O}_i)} \exp(\mathfrak{R}(\mathbf{v}^-, \mathbf{l}_i))},$$

where  $\mathbf{v}^{+/-} = \phi(o^{+/-})$ . Different pretraining strategies differ in their selection of (1) the positive frame set  $\mathcal{P}(\mathcal{O}_i)$ , (2) negative frame set  $\mathcal{N}(\mathcal{O}_i)$ ; and (3) the semantic alignment scoring function  $\mathfrak{R}(\mathbf{v}, \mathbf{l}_i)$  measuring the gap of VL similarities as detailed in Table 1.

**Discussion.** As motivated by goal-conditioned RL (Andrychowicz et al., 2017), current approaches *explicitly* select future frames (e.g., DecisionNCE) or the last frame (e.g., LIV) as the goal within the positive set, enforcing their visual embedding to align with the semantics. Likewise, the scoring functions  $\mathfrak{R}$  are often designed to maximize this transition direction. However, the pretraining action videos are *noisy* as actions may terminate early or include irrelevant subsequent actions, which may mislead the encoders and result in inaccurate vision-language association. As detecting precise action boundaries is non-trivial, we argue for a more flexible approach that leverages *intrinsic* characteristics of actions to guide pretraining.

## 4. Our Approach

We introduce an action temporal coherence learning (ACTOL) to capture two temporal properties of video actions: *ordering* and *continuity*. *Ordering* was ensured in the vision-language ordering loss (Section 4.1), where the semantic difference between frames reflects their temporal distance, with closer frames exhibiting smaller differences than those further apart. *Continuity* requires smooth visual transitions between adjacent frames, avoiding abrupt changes and high variance. To achieve this, we model sampled frame intervals as a Brownian bridge process (Section 4.2), penalizing deviations from the expected trajectories. Different from prior works that relies on setting explicit goal frames, the proposed approach *implicitly* explore the global and local structure of actions without imposing rigid constraints.

### 4.1. Visual-Language Ordering

To capture the temporal coherence of video actions, we first propose a vision-language ordering (VLO) loss that ensures the semantic alignment between frames reflects their temporal order. Consider an anchor frame  $o_i \in \mathcal{O}$  with an index  $n(i)$  corresponding to its position in the original video. For any given frame pair  $(o_i, o_j)$ , we first define the semantic alignment score  $\mathfrak{R}$  to quantify differences in their VL similarities *w.r.t* a language description  $l$  as:

$$\mathfrak{R}(\mathbf{v}_i, \mathbf{v}_j, \mathbf{l}) = -\|\text{sim}(\mathbf{v}_i, \mathbf{l}) - \text{sim}(\mathbf{v}_j, \mathbf{l})\|_2, \quad (1)$$

where  $\mathbf{v}_i = \phi(o_i)$ ,  $\mathbf{l} = \varphi(l)$ . The function  $\text{sim}(\cdot, \cdot)$  computes the VL similarity using cosine similarity. To ensure the proposed  $\mathfrak{R}$  adhere to the temporal ordering of frames, we construct a negative set  $\mathcal{N}_{i,j}$  by selecting  $o_k \in \mathcal{O}$  correspond to frames that are temporally more *distant* than the positive pair  $(o_i, o_j)$ :

$$\mathcal{N}_{i,j} = \{o_k \mid k \neq i, |n(i) - n(k)| \geq |n(i) - n(j)|\},$$

This formulation allows us to reformulate  $\mathcal{L}_{\text{tNCE}}$  by enforcing that the VL similarity difference between frames  $i$  and  $j$  should be smaller than that between frame  $i$  and any negative frame  $k$  within the video  $\mathcal{O}$ :

$$\mathcal{L}_{\text{VLO}} = -\mathbb{E}_{(o_i, o_j) \sim \mathcal{O}} \log \frac{\exp(\mathfrak{R}(\mathbf{v}_i, \mathbf{v}_j, \mathbf{l}))}{\sum_{o_k \in \mathcal{N}_{i,j}} \exp(\mathfrak{R}(\mathbf{v}_i, \mathbf{v}_k, \mathbf{l}))}.$$

Notably, our VLO loss does not strictly require  $o_j$  to be from future timestep for goal-reaching. Instead, we leverage the inherent temporal dynamics in videos, allowing the model to learn the natural ordering in an unsupervised manner with detailed analysis as follows.

**Theoretical Analysis.** Ordering and sorting properties are well-established in self-supervised learning (Shvetsova et al., 2023; Hu et al., 2021; Zha et al., 2023). Building upon these insights, we formalize the concept of vision-language ordering below.

**Definition 4.1** (Vision-Language Ordering). Let  $\{o_i\}_{i \in [T]}$  be a sequence of video frames and  $l$  the corresponding language description. The representations of the frames are said to satisfy the VLO property for any  $0 < \delta < 1$  if  $\forall i \in [T]$ , and distinct frames  $j, k \in [T] \setminus \{i\}$ , the following conditions hold:

$$\begin{cases} \mathfrak{R}_{i,j,l} > \mathfrak{R}_{i,k,l} + 1/\delta, & \text{if } d_{i,j} < d_{i,k}, \\ |\mathfrak{R}_{i,j,l} - \mathfrak{R}_{i,k,l}| < \delta, & \text{if } d_{i,j} = d_{i,k}, \\ \mathfrak{R}_{i,j,l} < \mathfrak{R}_{i,k,l} - 1/\delta, & \text{if } d_{i,j} > d_{i,k}, \end{cases}$$

where  $\mathfrak{R}_{i,j,l}$  denotes  $\mathfrak{R}(\mathbf{v}_i, \mathbf{v}_j, \mathbf{l})$  and the temporal distance between frames defined as  $|n(i) - n(j)|$  as  $d_{i,j}$ .

**Implications of the VLO Property.** The VLO property enforces a structured representation of video frames, ensuring that temporally adjacent frames have consistent and predictable semantic differences. When two frames have equal temporal distances from an anchor frame, their semantic gaps should be similar, fostering smooth transitions. In contrast, frames that are farther apart should exhibit larger semantic gaps, thus preserving the chronological order.

To formalize the temporal ordering constraints, we define the unique *sorted* set of frame distances from frame  $i$  as  $\{D_{i,1} < D_{i,2} < \dots < D_{i,M}\}$ , where each  $D_{i,m}$ ,  $m \in [M_i]$  is obtained by sorting the set  $\{d_{i,j} \mid j \in [T] \setminus \{i\}\}$ . Additionally, we define the count of frames at each distance level as:

$$n_{i,m} := |\{j \mid d_{i,j} = D_{i,m}, j \in [T] \setminus \{i\}\}|, \quad (2)$$

which denotes the number of frames whose temporal distance from frame  $i$  equals  $D_{i,m}$ . The VLO property is satisfied when the proposed  $\mathcal{L}_{\text{VLO}}$  approaches its theoretical lower bound, which is given by:

$$\mathcal{L}^* := \frac{1}{T(T-1)} \sum_{i=1}^T \sum_{m=1}^{M_i} n_{i,m} \log n_{i,m}. \quad (3)$$

This bound characterizes the optimal alignment of VL similarities, ensuring that the learned representations preserve the inherent temporal structure within the video sequence, as guaranteed by the following theorem.

**Theorem 4.2.**  $\mathcal{L}^*$  is a tight lower bound of  $\mathcal{L}_{\text{VLO}}$ , i.e.,  $\mathcal{L}_{\text{VLO}} \geq \mathcal{L}^*$ , and for any  $\epsilon > 0$ , there exists feature embeddings such that  $\mathcal{L}_{\text{VLO}} < \mathcal{L}^* + \epsilon$ . Furthermore, for any  $0 < \delta < 1$ , there exist  $\epsilon > 0$  such that if  $\mathcal{L}_{\text{VLO}} < \mathcal{L}^* + \epsilon$ , the learned representations satisfy the VLO property.

*Proof.* Please refer to Appendix A.1.  $\square$

### 4.2. Vision-Language Continuity

While the VLO property provides a strong global constraint on the structural alignment of VL pretraining, optimizing triplet relationships alone can be *unstable*. Variations



in frame content and noise often lead to *suboptimal* local consistency. To mitigate this, we introduce an additional local continuity constraint inspired by the *Brownian bridge* (Revuz & Yor, 2013). This stochastic process models transitions between two fixed endpoints over by any sampled local video interval  $[n(i), n(j)]$ . For any time step  $t \in [n(i), n(j)]$  within this interval, the transition density of Brownian Bridge process  $\mathbf{B}(t)$  follows a time-dependent Gaussian distribution:

$$\mathcal{N}\left(\mathbf{v}_i + \frac{t - n(i)}{n(j) - n(i)}(\mathbf{v}_j - \mathbf{v}_i), \frac{t(n(j) - n(i)) - t^2}{n(j) - n(i)}\right),$$

where  $\mathbf{v}_i, \mathbf{v}_j \in \mathbb{R}^d$  are the visual embeddings of the first and last frames in the sampled interval. The mean trajectory  $\mathbb{E}[\mathbf{B}(t)]$  linearly interpolates between the two endpoints, while the variance  $\text{Var}[\mathbf{B}(t)]$  peaks provides uncertainty modeling that peaks in the middle of the interval. To enforce this local continuity, the Brownian bridge loss  $\mathcal{L}_{\text{BB}}$  is formulated as,

$$\mathcal{L}_{\text{BB}} = \frac{1}{T} \sum_{t=1}^T \frac{1}{2\text{Var}[\mathbf{B}(t)]} \|\mathbf{v}_t - \mathbb{E}[\mathbf{B}(t)]\|_2^2. \quad (4)$$

This loss encourages local consistency by penalizing deviations from expected trajectories, ensuring consistency across short temporal spans.

**Overall Objective.** The final training objective integrates both global and local constraints to achieve temporal coherence simultaneously:

$$\mathcal{L}_{\text{ACTOL}} = \mathcal{L}_{\text{VLO}} + \lambda \mathcal{L}_{\text{BB}}, \quad (5)$$

where  $\lambda$  is empirically set to balance two components.

**Theoretical Analysis.** To provide a deeper understanding of continuity preservation, we present theoretical guarantee:

**Theorem 4.3** (Vision-Language Continuity). *Let  $\mathbf{v}_k, \mathbf{v}_l$  be arbitrary time step from the interval  $[n(i), n(j)]$  and  $\mathbf{l} \in \mathcal{L}$  be the language embedding. Suppose the VL similarity function  $\text{sim}(\cdot)$  is Lipschitz continuous with constant  $C$ . Assume that the frame embeddings are regularized by the Brownian Bridge constraint, then for any  $\epsilon > 0$ , there exists  $\delta > 0$  such that*

$$\|\mathbf{v}_k - \mathbf{v}_l\|_2 < \delta \Rightarrow |\mathfrak{R}(\mathbf{v}_k, \mathbf{v}_l, \mathbf{l})| < \epsilon.$$

*Proof.* Please refer to Appendix A.2.  $\square$

This theorem guarantees that under the Brownian Bridge constraint, if two video frames are temporally close, their semantic alignment score remains within a bounded range. This continuity can be further extended and show model resiliency to language perturbation:

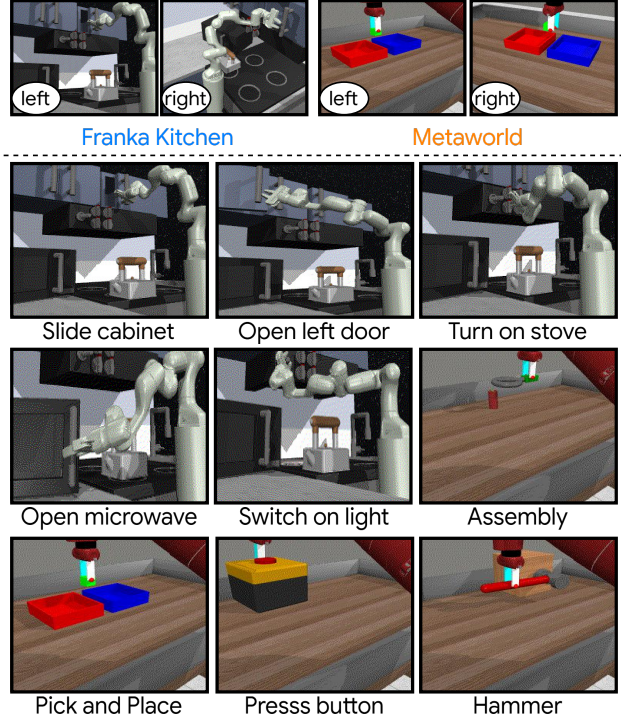


Figure 2. Simulation environments, including two camera views of Franka Kitchen (5 tasks) and Metaworld (4 tasks).

**Theorem 4.4** (Robustness to Language Variations). *Let  $\mathbf{l}'$  be the perturbed version of the original language embedding  $\mathbf{l}$  subject to a small constant  $\delta_l > 0$ , i.e.,  $\|\mathbf{l} - \mathbf{l}'\| \leq \delta_l$ , then the semantic alignment score  $\mathfrak{R}$  exhibits stability to the perturbation:*

$$|\mathfrak{R}(\mathbf{v}_i, \mathbf{v}_j, \mathbf{l}') - \mathfrak{R}(\mathbf{v}_i, \mathbf{v}_j, \mathbf{l})| \leq 2C\delta_l. \quad (6)$$

*Proof.* Please refer to Appendix A.3.  $\square$

Our empirical results, presented in Section 5.6, further validate these properties by showing improved generalization to varying linguistic instructions and more stable performance compared to baseline methods.

## 5. Experiment

**Experimental Setup.** We initialize our model with the weights of CLIP (Radford et al., 2021) with ResNet50 vision backbone and further pre-train it on the large-scale human action video dataset EPIC-KITCHEN-100 (Damen et al., 2018; 2020). For hyperparameter selection, we randomly sample 10 frames from each video per batch. The loss weight  $\lambda$  to 100. Other hyperparameters like temperatures follows the default value used in CLIP (Radford

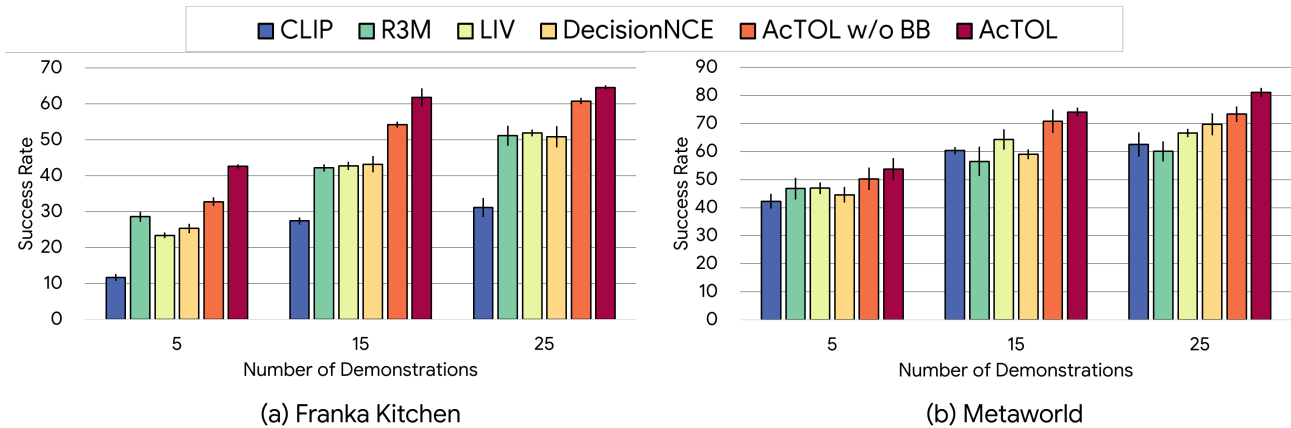


Figure 3. The averaged success rate comparisons over various tasks on (a) Franka Kitchen and (b) Metaworld.

et al., 2021). More pre-training details can be referred to Appendix B. In our experiments, we aim to evaluate the effectiveness of ordered and continuous vision-language representations for robotic control. First, we conduct extensive Language-Conditioned Behavior Cloning (LCBC) experiments in two different simulation environments to validate the importance of ordering and continuity for imitation learning. Second, we assess the utility of the learned representations as reward functions on multiple real-world action videos. The results demonstrate that the ordered and continuous representations enable our method to accurately identify action boundaries and generate dense rewards aligned with the given instructions. Finally, we evaluate the robustness of our method under language perturbations, showcasing its strong generalization capability for application in real-world daily scenarios.

### 5.1. Simulation Environments

We perform LCBC experiments in two widely used simulation environments for evaluation: **Franka Kitchen** (Gupta et al., 2019; Fu et al., 2020) and **Metaworld** (Yu et al., 2019). As shown in Figure 2, for Franka Kitchen, we evaluate five tasks: sliding a cabinet, opening the left door, opening the microwave, turning on the stove, and switching on the light. For Metaworld, we focus on learning four tasks: hammering a nail, pressing a button, picking and placing a block, and assembling a ring onto a peg. Detailed environment setup can be found at Appendix C.1.

In Frankakitchen, tasks often involve intricate actions that induce large visual changes, and the successful completion of these tasks requires precise, complex actions. As a result, tasks on FrankaKitchen rely more on visual trajectory representations. On the other hand, the visual scene in Metaworld is much simpler. Tasks on Metaworld generally involve direct actions with smaller visual changes, yet they require more sophisticated language understanding to act towards

specific task goals.

### 5.2. Baselines

Since our model is initialized with **CLIP** (Radford et al., 2021), a state-of-the-art image-text representation widely applied in various embodied tasks (Cui et al., 2022; Khandelwal et al., 2022; Shridhar et al., 2021; Tam et al., 2022), it is a natural choice to include CLIP as a vanilla baseline for comparison. Our primary baselines are **LIV** (Ma et al., 2023a) and **DecisionNCE** (Li et al., 2024), as we all use the same model architecture and dataset for pretraining. LIV employs the VIP (Ma et al., 2023b) to achieve consistent frame representations and aligns the final frame with instructions using the CLIP loss. DecisionNCE represents instructions as frame transitions and aligns the difference between the initial and final frames with the instructions using the CLIP loss. We also compare against **R3M** (Nair et al., 2022), pre-training on Ego4D (Grauman et al., 2022), which combines time contrastive learning (Sermanet et al., 2018) with LOReL (Nair et al., 2021) to ensure that later frames in the sequence receive higher rewards when aligned with the instruction.

### 5.3. Language-Conditioned Behavior Cloning

We keep the pre-trained vision-language encoders frozen and feed their output representations into a lightweight MLP to train the LCBC policies. Each task is performed from two camera viewpoints (left and right), with varying numbers of demonstrations [5, 15, 25] (*i.e.*, dataset size) for training, and evaluated under three different random seeds. We report the success rate across different environments and dataset sizes, averaged over camera views and seeds. Detailed comparison results can be referred to Appendix C.3.

Figure 3 presents the comparison results, showing that AcTOL significantly outperforms other methods across all

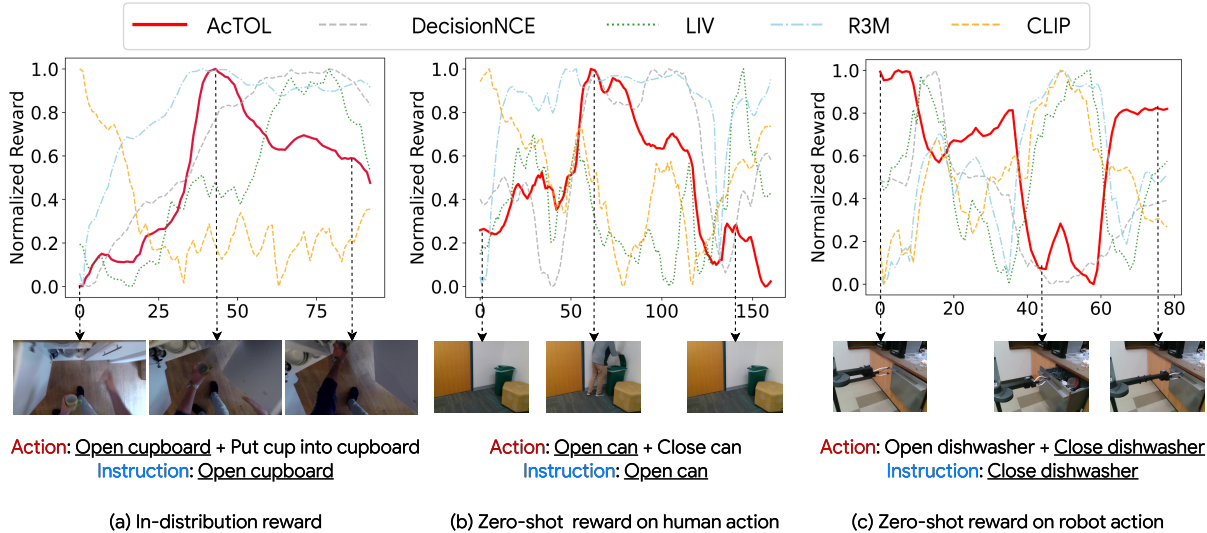


Figure 4. Visualization of the normalized learned reward corresponding to different actions. Our representations effectively help capture the correct temporal order of actions in the instruction. For more results, please refer to Appendix C.4.

dataset sizes in both environments, surpassing the SOTA by 49.0%/46.4%/26.3% and 14.6%/15.2%/16.3% at dataset sizes of 5/15/25, respectively, which demonstrates the effectiveness of our pre-training strategy. Especially in Franka Kitchen, where complex tasks demand higher action continuity, our method demonstrates a clear advantage with limited data, highlighting its superior data efficiency and low-resource generalization capability. Among the baseline models, CLIP consistently shows lower performance, particularly for Franka Kitchen. This indicates that while it excels in image representation, its inability to capture temporal characteristics in videos leads to suboptimal results in control tasks. R3M, LIV, and DecisionNCE perform well in the FrankaKitchen environment, but R3M shows a significant drop in performance in Metaworld. This discrepancy stems from R3M’s design, which utilizes a frozen language encoder to generate language features as conditions. These features are then used to optimize the visual encoder by maximizing the reward for temporally later frames. This approach results in a shortcut that prioritizes maximizing temporal visual differences rather than genuinely aligning visual representations with language semantics. This limitation is particularly evident in Franka Kitchen, where large visual changes dominate, allowing R3M to excel despite its lack of true language-visual alignment. In contrast, LIV and DecisionNCE employ CLIP-based losses during pre-training on video data, enabling them to align visual changes with semantics. This capability allows them to maintain solid performance even in Metaworld, where tasks require more refined language comprehension to interpret subtle visual changes. However, both models suffer from rigid assumptions about action semantics during pre-training, resulting in suboptimal alignment between vision and instructions.

Notably, when using 5/15 demonstrations, our method achieves results that are *comparable* to, or even *surpass*, those of other methods using 15/25 demonstrations, illustrating that our approach can utilize expert data more effectively. This is particularly advantageous when collecting expert data is time-consuming and labor-intensive. Moreover, when the Brownian Bridge constraint is not applied, although our method still outperforms the other baselines, its performance decreases noticeably. This indicates that the Brownian Bridge constraint effectively improves the quality of learned representations, leading to better policy optimization in behavior cloning.

#### 5.4. Language-Conditioned Visual Rewards

Since our model learns semantically smooth visual representations, the resulting semantic trajectories can also serve as ideal task rewards. Specifically, we define the reward at time step  $i$  as  $\cos(\mathbf{v}^i, \mathbf{l})$ , which reflects the distance between the current state and the language goal. Previous works (Ma et al., 2023a; Li et al., 2024) have primarily tested their rewards on single-action video clips. To increase task complexity, we selected three video clips, each containing two consecutive actions, to better evaluate whether the model accurately understands action semantics. We present more reward results in Appendix C.4. Figure 4 shows the actions, the instructions given and the corresponding reward curves. Figure 4(a) uses a video from EPIC-KITCHEN-100 to evaluate the effectiveness of in-distribution rewards. Our method produces an ideal reward curve, starting at a low point and reaching a peak as the action “open cupboard” completes, before declining as subsequent actions begin. In contrast, we observe that the rewards generated by R3M



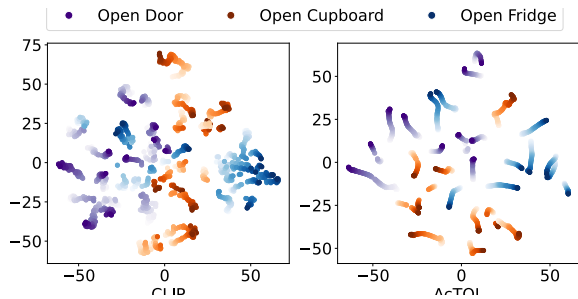


Figure 5. Visualization of visual trajectory representations.

and DecisionNCE continue to rise even after the “open cupboard” action has finished. This indicates that their training methodologies fail to effectively distinguish between actions that align with the instruction and those that do not. Figure 4(b) and (c) evaluate the reward generation capabilities in real-world scenarios using two videos from (Bahl et al., 2022). These videos involve humans and robots consecutively performing pairs of opposite actions. It is evident that only our method is capable of generating the correct reward curve, accurately identifying the start and end of the actions specified by the instruction, and producing opposite rewards for contrasting actions. This demonstrates that our method, by learning ordered and continuous vision-language representations, inherently captures the trends of semantic changes in actions. It effectively aligns visual trajectories with the corresponding instructions, highlighting its significant potential as a language-conditioned visual reward model.

### 5.5. Visualization of Visual Representation Trajectory

To demonstrate the smoothness of the representations, we select three distinct language instructions from the EPIC-KITCHEN-100 dataset, each corresponding to 10 action videos. We then visualize the visual representations learned by our method and those by CLIP using t-SNE (van der Maaten & Hinton, 2008), as shown in Figure 5. The representations produced by CLIP show clear separability between different language instructions, and the trajectories of individual videos maintain a certain degree of temporal consistency. However, the transitions between consecutive frames are not smooth, reflecting a flaw due to the absence of training on video data. In contrast, our method significantly enhances the ordering and continuity of video feature trajectories while preserving the discriminative power of CLIP for distinguishing actions associated with different instructions. This improvement stems from training directly on CLIP’s weights and optimizing the temporal consistency within each video. As a result, our method not only achieves smoother representations but also retains the strong alignment between visual features and language semantics inherent in CLIP’s original design. This balance between

Table 2. Success rate fluctuation under linguistic perturbations on Franka Kitchen.

| Task            | LIV             | DecisionNCE    | AcTOL          |
|-----------------|-----------------|----------------|----------------|
| Slide Cabinet   | $-29.0 \pm 3.0$ | $-4.5 \pm 3.5$ | $1.0 \pm 2.0$  |
| Open Left Door  | $-3.5 \pm 0.5$  | $-1.5 \pm 1.5$ | $1.0 \pm 2.0$  |
| Open Microwave  | $-4.5 \pm 0.5$  | $3.0 \pm 2.0$  | $-2.5 \pm 1.5$ |
| Turn on stove   | $-8.5 \pm 0.5$  | $-6.5 \pm 1.5$ | $-0.5 \pm 1.5$ |
| Switch on light | $-12.5 \pm 0.5$ | $-1.0 \pm 3.0$ | $1.0 \pm 1.0$  |
| Average         | $-11.6 \pm 0.6$ | $-2.1 \pm 0.3$ | $0.2 \pm 1.6$  |

temporal coherence and semantic distinctiveness highlights the effectiveness of our approach in refining embodied representations for tasks requiring nuanced understanding of multimodal alignment and temporal dynamics.

### 5.6. Robustness Study under Linguistic Perturbations

In the EPIC-KITCHEN-100 dataset, textual annotations are often concise, such as “open cupboard”. In the default setting of LCBC, we employ similarly structured simple instructions. In this experiment, to validate the robustness of the representations our method learns in real-world scenarios, we introduce minor modifications to the language instructions. Specifically, we transform the original instruction “{action}” into two more conversational styles, *i.e.*, “Please {action} for me.” and “Help me {action}.”. We then evaluate the imitation learning performance conditioned on these modified instructions in the Franka Kitchen environment. For comparison, we select LIV and DecisionNCE, which are also pre-trained on EPIC-KITCHEN-100. As shown in Table 2, The success rates of LIV and DecisionNCE dropped by 11.6% and 2.1%, respectively, whereas our method maintained a success rate comparable to that before the language perturbation. This result demonstrates the robustness of our learned representations, which generalize more effectively to real-world scenarios.

## 6. Conclusion

We present Action Temporal Coherence Learning (AcTOL) as a promising vision-language pre-training solution for generalizable embodied agents. By learning action consistency from a large corpus of human action videos, AcTOL theoretically ensures the ordering and continuity of vision-language representations, as well as robustness to language perturbations. Extensive experiments across various environments demonstrate that AcTOL effectively generalizes to complex robotic manipulation tasks. Due to hardware limitations, our evaluations are mainly conducted in simulation environments, with real-world deployment left for future work.



## 7. Impact Statement

This paper aims to advance the development of Embodied AI. A potential ethical concern is that large-scale data used for vision-language representation pre-training may inadvertently contain sensitive information or biases. To address this, we use the publicly available and rigorously reviewed EPIC-KITCHEN-100 human action video dataset (Damen et al., 2018; 2020) in our experiments to ensure compliance with ethical standards.

## References

- Andrychowicz, M., Crow, D., Ray, A., Schneider, J., Fong, R., Welinder, P., McGrew, B., Tobin, J., Abbeel, P., and Zaremba, W. Hindsight experience replay. In Guyon, I., von Luxburg, U., Bengio, S., Wallach, H. M., Fergus, R., Vishwanathan, S. V. N., and Garnett, R. (eds.), *Advances in Neural Information Processing Systems 30: Annual Conference on Neural Information Processing Systems, (NeurIPS)*, pp. 5048–5058, 2017.
- Bahl, S., Gupta, A., and Pathak, D. Human-to-robot imitation in the wild. In Hauser, K., Shell, D. A., and Huang, S. (eds.), *Robotics: Science and Systems XVIII, New York City, NY, USA, June 27 - July 1, 2022*, 2022.
- Brown, T. B., Mann, B., Ryder, N., Subbiah, M., Kaplan, J., Dhariwal, P., Neelakantan, A., Shyam, P., Sastry, G., Askell, A., Agarwal, S., Herbert-Voss, A., Krueger, G., Henighan, T., Child, R., Ramesh, A., Ziegler, D. M., Wu, J., Winter, C., Hesse, C., Chen, M., Sigler, E., Litwin, M., Gray, S., Chess, B., Clark, J., Berner, C., McCandlish, S., Radford, A., Sutskever, I., and Amodei, D. Language models are few-shot learners. In Larochelle, H., Ranzato, M., Hadsell, R., Balcan, M., and Lin, H. (eds.), *Advances in Neural Information Processing Systems 33: Annual Conference on Neural Information Processing Systems, (NeurIPS)*, 2020.
- Cheang, C., Chen, G., Jing, Y., Kong, T., Li, H., Li, Y., Liu, Y., Wu, H., Xu, J., Yang, Y., Zhang, H., and Zhu, M. GR-2: A generative video-language-action model with web-scale knowledge for robot manipulation. *CoRR*, abs/2410.06158, 2024.
- Collaboration, O. X., Padalkar, A., Pooley, A., Jain, A., Bewley, A., Herzog, A., Irpan, A., Khazatsky, A., Raj, A., Singh, A., Brohan, A., Raffin, A., Wahid, A., Burgess-Limerick, B., Kim, B., Schölkopf, B., Ichter, B., Lu, C., Xu, C., Finn, C., Xu, C., Chi, C., Huang, C., Chan, C., Pan, C., Fu, C., Devin, C., Driess, D., Pathak, D., Shah, D., Büchler, D., Kalashnikov, D., Sadigh, D., Johns, E., Ceola, F., Xia, F., Stulp, F., Zhou, G., Sukhatme, G. S., Salhotra, G., Yan, G., Schiavi, G., Kahn, G., Su, H., Fang, H., Shi, H., Amor, H. B., Christensen, H. I., Furuta, H., Walke, H., Fang, H., Mordatch, I., Radosavovic, I., and et al. Open x-embodiment: Robotic learning datasets and RT-X models. *CoRR*, abs/2310.08864, 2023.
- Cui, Y., Niekum, S., Gupta, A., Kumar, V., and Rajeswaran, A. Can foundation models perform zero-shot task specification for robot manipulation? In Firoozi, R., Mehr, N., Yel, E., Antonova, R., Bohg, J., Schwager, M., and Kochenderfer, M. J. (eds.), *Learning for Dynamics and Control Conference, (LADC)*, volume 168 of *Proceedings of Machine Learning Research*, pp. 893–905. PMLR, 2022.
- Damen, D., Doughty, H., Farinella, G. M., Fidler, S., Furnari, A., Kazakos, E., Moltisanti, D., Munro, J., Perrett, T., Price, W., and Wray, M. Scaling egocentric vision: The EPIC-KITCHENS dataset. *CoRR*, abs/1804.02748, 2018.
- Damen, D., Doughty, H., Farinella, G. M., Furnari, A., Kazakos, E., Ma, J., Moltisanti, D., Munro, J., Perrett, T., Price, W., and Wray, M. Rescaling egocentric vision. *CoRR*, abs/2006.13256, 2020.
- Fu, J., Kumar, A., Nachum, O., Tucker, G., and Levine, S. D4RL: datasets for deep data-driven reinforcement learning. *CoRR*, abs/2004.07219, 2020.
- Goyal, R., Kahou, S. E., Michalski, V., Materzynska, J., Westphal, S., Kim, H., Haenel, V., Fründ, I., Yianilos, P., Mueller-Freitag, M., Hoppe, F., Thureau, C., Bax, I., and Memisevic, R. The ”something something” video database for learning and evaluating visual common sense. In *IEEE International Conference on Computer Vision, ICCV 2017, Venice, Italy, October 22-29, 2017*, pp. 5843–5851. IEEE Computer Society, 2017.
- Grauman, K., Westbury, A., Byrne, E., Chavis, Z., Furnari, A., Girdhar, R., Hamburger, J., Jiang, H., Liu, M., Liu, X., Martin, M., Nagarajan, T., Radosavovic, I., Ramakrishnan, S. K., Ryan, F., Sharma, J., Wray, M., Xu, M., Xu, E. Z., Zhao, C., Bansal, S., Batra, D., Cartillier, V., Crane, S., Do, T., Doulaty, M., Erapalli, A., Feichtenhofer, C., Fragomeni, A., Fu, Q., Gebreselasie, A., González, C., Hillis, J., Huang, X., Huang, Y., Jia, W., Khoo, W., Kolár, J., Kottur, S., Kumar, A., Landini, F., Li, C., Li, Y., Li, Z., Mangalam, K., Modhugu, R., Munro, J., Murrell, T., Nishiyasu, T., Price, W., Puentes, P. R., Ramazanov, M., Sari, L., Somasundaram, K., Southerland, A., Sugano, Y., Tao, R., Vo, M., Wang, Y., Wu, X., Yagi, T., Zhao, Z., Zhu, Y., Arbeláez, P., Crandall, D., Damen, D., Farinella, G. M., Fuegen, C., Ghanem, B., Ithapu, V. K., Jawahar, C. V., Joo, H., Kitani, K., Li, H., Newcombe, R. A., Oliva, A., Park, H. S., Rehg, J. M., Sato, Y., Shi, J., Shou, M. Z., Torralba, A., Torresani, L., Yan, M., and Malik, J. Ego4d: Around the world in 3, 000 hours of egocentric video. In

- IEEE/CVF Conference on Computer Vision and Pattern Recognition, (CVPR)*, pp. 18973–18990. IEEE, 2022.
- Gupta, A., Kumar, V., Lynch, C., Levine, S., and Hausman, K. Relay policy learning: Solving long-horizon tasks via imitation and reinforcement learning. In Kaelbling, L. P., Kragic, D., and Sugiura, K. (eds.), *3rd Annual Conference on Robot Learning, (CoRL)*, volume 100 of *Proceedings of Machine Learning Research*, pp. 1025–1037. PMLR, 2019.
- He, K., Zhang, X., Ren, S., and Sun, J. Deep residual learning for image recognition. In *2016 IEEE Conference on Computer Vision and Pattern Recognition, (CVPR)*, pp. 770–778. IEEE Computer Society, 2016.
- Hu, K., Shao, J., Liu, Y., Raj, B., Savvides, M., and Shen, Z. Contrast and order representations for video self-supervised learning. In *2021 IEEE/CVF International Conference on Computer Vision, ICCV 2021, Montreal, QC, Canada, October 10-17, 2021*, pp. 7919–7929. IEEE, 2021. doi: 10.1109/ICCV48922.2021.00784. URL <https://doi.org/10.1109/ICCV48922.2021.00784>.
- Karamcheti, S., Nair, S., Chen, A. S., Kollar, T., Finn, C., Sadigh, D., and Liang, P. Language-driven representation learning for robotics. In Bekris, K. E., Hauser, K., Herbert, S. L., and Yu, J. (eds.), *Robotics: Science and Systems XIX, (RSS)*, 2023.
- Khandelwal, A., Weihs, L., Mottaghi, R., and Kembhavi, A. Simple but effective: CLIP embeddings for embodied AI. In *IEEE/CVF Conference on Computer Vision and Pattern Recognition, (CVPR)*, pp. 14809–14818. IEEE, 2022.
- Kim, M. J., Pertsch, K., Karamcheti, S., Xiao, T., Balakrishna, A., Nair, S., Rafailov, R., Foster, E. P., Lam, G., Sanketi, P., Vuong, Q., Kollar, T., Burchfiel, B., Tedrake, R., Sadigh, D., Levine, S., Liang, P., and Finn, C. Openvla: An open-source vision-language-action model. *CoRR*, abs/2406.09246, 2024.
- Li, J., Zheng, J., Zheng, Y., Mao, L., Hu, X., Cheng, S., Niu, H., Liu, J., Liu, Y., Liu, J., Zhang, Y., and Zhan, X. Decisionncc: Embodied multimodal representations via implicit preference learning. In *Forty-first International Conference on Machine Learning, (ICML)*. OpenReview.net, 2024.
- Liu, H., Li, C., Wu, Q., and Lee, Y. J. Visual instruction tuning. In Oh, A., Naumann, T., Globerson, A., Saenko, K., Hardt, M., and Levine, S. (eds.), *Advances in Neural Information Processing Systems 36: Annual Conference on Neural Information Processing Systems, (NeurIPS)*, 2023.
- Liu, Y., Chen, W., Bai, Y., Li, G., Gao, W., and Lin, L. Aligning cyber space with physical world: A comprehensive survey on embodied AI. *CoRR*, abs/2407.06886, 2024. doi: 10.48550/ARXIV.2407.06886. URL <https://doi.org/10.48550/arXiv.2407.06886>.
- Ma, Y. J., Kumar, V., Zhang, A., Bastani, O., and Jayaraman, D. LIV: language-image representations and rewards for robotic control. In Krause, A., Brunskill, E., Cho, K., Engelhardt, B., Sabato, S., and Scarlett, J. (eds.), *International Conference on Machine Learning, (ICML)*, volume 202 of *Proceedings of Machine Learning Research*, pp. 23301–23320. PMLR, 2023a.
- Ma, Y. J., Sodhani, S., Jayaraman, D., Bastani, O., Kumar, V., and Zhang, A. VIP: towards universal visual reward and representation via value-implicit pre-training. In *The Eleventh International Conference on Learning Representations, (ICLR)*. OpenReview.net, 2023b.
- Majumdar, A., Yadav, K., Arnaud, S., Ma, Y. J., Chen, C., Silwal, S., Jain, A., Berges, V., Wu, T., Vakil, J., Abbeel, P., Malik, J., Batra, D., Lin, Y., Maksymets, O., Rajeswaran, A., and Meier, F. Where are we in the search for an artificial visual cortex for embodied intelligence? In Oh, A., Naumann, T., Globerson, A., Saenko, K., Hardt, M., and Levine, S. (eds.), *Advances in Neural Information Processing Systems 36: Annual Conference on Neural Information Processing Systems 2023, (NeurIPS)*, 2023.
- Mu, Y., Zhang, Q., Hu, M., Wang, W., Ding, M., Jin, J., Wang, B., Dai, J., Qiao, Y., and Luo, P. Embodiedgpt: Vision-language pre-training via embodied chain of thought. In Oh, A., Naumann, T., Globerson, A., Saenko, K., Hardt, M., and Levine, S. (eds.), *Advances in Neural Information Processing Systems (NeurIPS)*, 2023.
- Nair, S., Mitchell, E., Chen, K., Ichter, B., Savarese, S., and Finn, C. Learning language-conditioned robot behavior from offline data and crowd-sourced annotation. In Faust, A., Hsu, D., and Neumann, G. (eds.), *Conference on Robot Learning, (CoRL)*, volume 164 of *Proceedings of Machine Learning Research*, pp. 1303–1315. PMLR, 2021.
- Nair, S., Rajeswaran, A., Kumar, V., Finn, C., and Gupta, A. R3M: A universal visual representation for robot manipulation. In Liu, K., Kulic, D., and Ichnowski, J. (eds.), *Conference on Robot Learning, (CoRL)*, volume 205 of *Proceedings of Machine Learning Research*, pp. 892–909. PMLR, 2022.
- Radford, A., Kim, J. W., Hallacy, C., Ramesh, A., Goh, G., Agarwal, S., Sastry, G., Askell, A., Mishkin, P., Clark, J., Krueger, G., and Sutskever, I. Learning transferable visual models from natural language supervision. In Meila,

- M. and Zhang, T. (eds.), *Proceedings of the 38th International Conference on Machine Learning, (ICML)*, volume 139 of *Proceedings of Machine Learning Research*, pp. 8748–8763. PMLR, 2021.
- Radosavovic, I., Xiao, T., James, S., Abbeel, P., Malik, J., and Darrell, T. Real-world robot learning with masked visual pre-training. In Liu, K., Kulic, D., and Ichnowski, J. (eds.), *Conference on Robot Learning, (CoRL)*, volume 205 of *Proceedings of Machine Learning Research*, pp. 416–426. PMLR, 2022.
- Revuz, D. and Yor, M. *Continuous martingales and Brownian motion*, volume 293. Springer Science & Business Media, 2013.
- Sermanet, P., Lynch, C., Chebotar, Y., Hsu, J., Jang, E., Schaal, S., and Levine, S. Time-contrastive networks: Self-supervised learning from video. In *2018 IEEE International Conference on Robotics and Automation, (ICRA)*, pp. 1134–1141. IEEE, 2018.
- Shridhar, M., Manuelli, L., and Fox, D. Cliport: What and where pathways for robotic manipulation. In Faust, A., Hsu, D., and Neumann, G. (eds.), *Conference on Robot Learning, (CoRL)*, volume 164 of *Proceedings of Machine Learning Research*, pp. 894–906. PMLR, 2021.
- Shvetsova, N., Petersen, F., Kukleva, A., Schiele, B., and Kuehne, H. Learning by sorting: Self-supervised learning with group ordering constraints. In *IEEE/CVF International Conference on Computer Vision, ICCV 2023, Paris, France, October 1-6, 2023*, pp. 16407–16417. IEEE, 2023. doi: 10.1109/ICCV51070.2023.01508. URL <https://doi.org/10.1109/ICCV51070.2023.01508>.
- Tam, A. C., Rabinowitz, N. C., Lampinen, A. K., Roy, N. A., Chan, S. C. Y., Strouse, D., Wang, J., Banino, A., and Hill, F. Semantic exploration from language abstractions and pretrained representations. In Koyejo, S., Mohamed, S., Agarwal, A., Belgrave, D., Cho, K., and Oh, A. (eds.), *Advances in Neural Information Processing Systems 35: Annual Conference on Neural Information Processing Systems 2022, (NeurIPS)*, 2022.
- van der Maaten, L. and Hinton, G. Visualizing data using t-sne. *Journal of Machine Learning Research*, 2008.
- Ye, S., Jang, J., Jeon, B., Joo, S. J., Yang, J., Peng, B., Mandekar, A., Tan, R., Chao, Y., Lin, B. Y., Liden, L., Lee, K., Gao, J., Zettlemoyer, L., Fox, D., and Seo, M. Latent action pretraining from videos. *CoRR*, abs/2410.11758, 2024.
- Yu, T., Quillen, D., He, Z., Julian, R., Hausman, K., Finn, C., and Levine, S. Meta-world: A benchmark and evaluation for multi-task and meta reinforcement learning. In Kaelbling, L. P., Kragic, D., and Sugiura, K. (eds.), *3rd Annual Conference on Robot Learning, (CoRL)*, volume 100 of *Proceedings of Machine Learning Research*, pp. 1094–1100. PMLR, 2019.
- Zeng, J., Bu, Q., Wang, B., Xia, W., Chen, L., Dong, H., Song, H., Wang, D., Hu, D., Luo, P., Cui, H., Zhao, B., Li, X., Qiao, Y., and Li, H. Learning manipulation by predicting interaction. *CoRR*, abs/2406.00439, 2024.
- Zha, K., Cao, P., Son, J., Yang, Y., and Katabi, D. Rank-n-contrast: Learning continuous representations for regression. In Oh, A., Naumann, T., Globerson, A., Saenko, K., Hardt, M., and Levine, S. (eds.), *Advances in Neural Information Processing Systems 36: Annual Conference on Neural Information Processing Systems 2023, (NeurIPS)*, LA, USA, December 10 - 16, 2023, 2023.
- Zitkovich, B., Yu, T., Xu, S., Xu, P., Xiao, T., Xia, F., Wu, J., Wohlhart, P., Welker, S., Wahid, A., Vuong, Q., Vanhoucke, V., Tran, H. T., Soricut, R., Singh, A., Singh, J., Sermanet, P., Sanketi, P. R., Salazar, G., Ryoo, M. S., Reymann, K., Rao, K., Pertsch, K., Mordatch, I., Michalewski, H., Lu, Y., Levine, S., Lee, L., Lee, T. E., Leal, I., Kuang, Y., Kalashnikov, D., Julian, R., Joshi, N. J., Irpan, A., Ichter, B., Hsu, J., Herzog, A., Hausman, K., Gopalakrishnan, K., Fu, C., Florence, P., Finn, C., Dubey, K. A., Driess, D., Ding, T., Choromanski, K. M., Chen, X., Chebotar, Y., Carbajal, J., Brown, N., Brohan, A., Arenas, M. G., and Han, K. RT-2: vision-language-action models transfer web knowledge to robotic control. In Tan, J., Toussaint, M., and Darvish, K. (eds.), *Conference on Robot Learning, (CoRL)*, volume 229 of *Proceedings of Machine Learning Research*, pp. 2165–2183. PMLR, 2023.

## A. Proofs

### A.1. Proofs of Theorem 4.2

For the proof of Theorem 4.2, we closely follow the approaches presented in (Zha et al., 2023) and adapted to our triplet case. We prove the theorem in three steps:

(1)  $\mathcal{L}^* := \frac{1}{T(T-1)} \sum_{i=1}^T \sum_{m=1}^{M_i} n_{i,m} \log n_{i,m}$  is a lower bound of  $\mathcal{L}_{\text{VLO}}$ , i.e.,  $\mathcal{L}_{\text{VLO}} > \mathcal{L}^*$ .

(2)  $\mathcal{L}^*$  is tight, i.e., for any  $\epsilon > 0$ , there exists representations such that  $\mathcal{L}_{\text{VLO}} < \mathcal{L}^* + \epsilon$ .

(3) For any  $0 < \delta < 1$ , there exist  $\epsilon > 0$ , such that if  $\mathcal{L}_{\text{VLO}} < \mathcal{L}^* + \epsilon$ , then the learned representations satisfy VLO property.

(1) Recall that  $\mathcal{L}_{\text{VLO}} = \frac{1}{T} \sum_{i=1}^T \frac{1}{T-1} \sum_{j=1, j \neq i}^T -\log \frac{\exp(\mathfrak{R}_{i,j,l})}{\sum_{\mathbf{v}_k \in \mathcal{N}_{i,j}} \exp(\mathfrak{R}_{i,k,l})}$ , where  $\mathcal{N}_{i,j} = \{\mathbf{v}_k | k \neq i, d_{i,j} < d_{i,k}\}$ , we rewrite it as

$$\begin{aligned}
 \mathcal{L}_{\text{VLO}} &= -\frac{1}{T(T-1)} \sum_{i=1}^T \sum_{j \in [T] \setminus \{i\}} \log \frac{\exp(\mathfrak{R}_{i,j,l})}{\sum_{k \in [T] \setminus \{i\}, d_{i,k} \geq d_{i,j}} \exp(\mathfrak{R}_{i,k,l})} \\
 &= -\frac{1}{T(T-1)} \sum_{i=1}^T \sum_{m=1}^{M_i} \sum_{j \in [T] \setminus \{i\}, d_{i,j} = D_{i,m}} \log \frac{\exp(\mathfrak{R}_{i,j,l})}{\sum_{k \in [T] \setminus \{i\}, d_{i,k} \geq D_{i,m}} \exp(\mathfrak{R}_{i,k,l})} \\
 &= -\frac{1}{T(T-1)} \sum_{i=1}^T \sum_{m=1}^{M_i} \sum_{j \in [T] \setminus \{i\}, d_{i,j} = D_{i,m}} \log \frac{1}{\sum_{k \in [T] \setminus \{i\}, d_{i,k} \geq D_{i,m}} \exp(\mathfrak{R}_{i,k,l} - \mathfrak{R}_{i,j,l})} \\
 &= -\frac{1}{T(T-1)} \sum_{i=1}^T \sum_{m=1}^{M_i} \sum_{j \in [T] \setminus \{i\}, d_{i,j} = D_{i,m}} \log \frac{1}{\sum_{k \in [T] \setminus \{i\}, d_{i,k} = D_{i,m}} \exp(\mathfrak{R}_{i,k,l} - \mathfrak{R}_{i,j,l})} \\
 &\quad - \frac{1}{T(T-1)} \sum_{i=1}^T \sum_{m=1}^{M_i} \sum_{j \in [T] \setminus \{i\}, d_{i,j} = D_{i,m}} \log \frac{\sum_{k \in [T] \setminus \{i\}, d_{i,k} = D_{i,m}} \exp(\mathfrak{R}_{i,k,l} - \mathfrak{R}_{i,j,l})}{\sum_{k \in [T] \setminus \{i\}, d_{i,k} \geq D_{i,m}} \exp(\mathfrak{R}_{i,k,l} - \mathfrak{R}_{i,j,l})} \\
 &= -\frac{1}{T(T-1)} \sum_{i=1}^T \sum_{m=1}^{M_i} \sum_{j \in [T] \setminus \{i\}, d_{i,j} = D_{i,m}} \log \frac{\exp(\mathfrak{R}_{i,j,l})}{\sum_{k \in [T] \setminus \{i\}, d_{i,k} = D_{i,m}} \exp(\mathfrak{R}_{i,k,l})} \\
 &\quad + \frac{1}{T(T-1)} \sum_{i=1}^T \sum_{m=1}^{M_i} \sum_{j \in [T] \setminus \{i\}, d_{i,j} = D_{i,m}} \log \left( 1 + \frac{\sum_{k \in [T] \setminus \{i\}, d_{i,k} > D_{i,m}} \exp(\mathfrak{R}_{i,k,l} - \mathfrak{R}_{i,j,l})}{\sum_{k \in [T] \setminus \{i\}, d_{i,k} = D_{i,m}} \exp(\mathfrak{R}_{i,k,l} - \mathfrak{R}_{i,j,l})} \right) \\
 &> -\frac{1}{T(T-1)} \sum_{i=1}^T \sum_{m=1}^{M_i} \sum_{j \in [T] \setminus \{i\}, d_{i,j} = D_{i,m}} \log \frac{\exp(\mathfrak{R}_{i,j,l})}{\sum_{k \in [T] \setminus \{i\}, d_{i,k} = D_{i,m}} \exp(\mathfrak{R}_{i,k,l})}.
 \end{aligned} \tag{7}$$

$\forall i \in [T], m \in [M_i]$ , from Jensen's Inequality we have

$$\begin{aligned}
 & - \sum_{j \in [T] \setminus \{i\}, d_{i,j} = D_{i,m}} \log \frac{\exp(\mathfrak{R}_{i,j,l})}{\sum_{k \in [T] \setminus \{i\}, d_{i,k} = D_{i,m}} \exp(\mathfrak{R}_{i,k,l})} \\
 & \geq -n_{i,m} \log \left( \frac{1}{n_{i,m}} \sum_{j \in [T] \setminus \{i\}, d_{i,j} = D_{i,m}} \frac{\exp(\mathfrak{R}_{i,j,l})}{\sum_{k \in [T] \setminus \{i\}, d_{i,k} = D_{i,m}} \exp(\mathfrak{R}_{i,k,l})} \right) = n_{i,m} \log n_{i,m}.
 \end{aligned} \tag{8}$$

Thus, by plugging Eq. (8) into Eq. (7), we have



$$\mathcal{L}_{\text{VLO}} > \frac{1}{T(T-1)} \sum_{i=1}^T \sum_{m=1}^{M_i} n_{i,m} \log n_{i,m} = L^* \quad (9)$$

(2) We will show for  $\forall \epsilon > 0$ , there is a set of representations where

$$\begin{cases} \mathfrak{R}_{i,j,l} > \mathfrak{R}_{i,k,l} + \gamma \text{ if } d_{i,j} < d_{i,k} \\ \mathfrak{R}_{i,j,l} = \mathfrak{R}_{i,k,l} \text{ if } d_{i,j} = d_{i,k} \end{cases}$$

and  $\gamma := \log \frac{T}{\min_{i \in [T], m \in [M_i]} n_{i,m} \epsilon}$ ,  $\forall i \in [T], j, k \in [T] \setminus \{i\}$ , such that  $\mathcal{L}_{\text{VLO}} < L^* + \epsilon$ . For such a set of representations,  $\forall i \in [T], m \in [M_i], j \in \{[T] \setminus \{i\} \mid d_{i,j} = D_{i,m}\}$ ,

$$-\log \frac{\exp(\mathfrak{R}_{i,j,l})}{\sum_{k \in [T] \setminus \{i\}, d_{i,k} = D_{i,m}} \exp(\mathfrak{R}_{i,k,l})} = \log n_{i,m} \quad (10)$$

since  $\mathfrak{R}_{i,k,l} = \mathfrak{R}_{i,j,l}$  for all  $k$  such that  $d_{i,k} = D_{i,m} = d_{i,j}$ , and

$$\begin{aligned} & \log \left( 1 + \frac{\sum_{k \in [T] \setminus \{i\}, d_{i,k} > D_{i,m}} \exp(\mathfrak{R}_{i,k,l} - \mathfrak{R}_{i,j,l})}{\sum_{k \in [T] \setminus \{i\}, d_{i,k} = D_{i,m}} \exp(\mathfrak{R}_{i,k,l} - \mathfrak{R}_{i,j,l})} \right) \\ & < \log \left( 1 + \frac{T \exp(-\gamma)}{n_{i,m}} \right) < \frac{T \exp(-\gamma)}{n_{i,m}} \leq \epsilon. \end{aligned} \quad (11)$$

As  $\mathfrak{R}_{i,k,l} - \mathfrak{R}_{i,j,l} < -\gamma$  for all  $k$  such that  $d_{i,k} > D_{i,m} = d_{i,j}$  and  $\mathfrak{R}_{i,k,l} - \mathfrak{R}_{i,j,l} = 0$  for all  $k$  such that  $d_{i,k} = D_{i,m} = d_{i,j}$ . From Eq. (7) we have

$$\begin{aligned} \mathcal{L}_{\text{VLO}} &= -\frac{1}{T(T-1)} \sum_{i=1}^T \sum_{m=1}^{M_i} \sum_{j \in [T] \setminus \{i\}, d_{i,j} = D_{i,m}} \log \frac{\exp(\mathfrak{R}_{i,j,l})}{\sum_{k \in [T] \setminus \{i\}, d_{i,k} = D_{i,m}} \exp(\mathfrak{R}_{i,k,l})} \\ &+ \frac{1}{T(T-1)} \sum_{i=1}^T \sum_{m=1}^{M_i} \sum_{j \in [T] \setminus \{i\}, d_{i,j} = D_{i,m}} \log \left( 1 + \frac{\sum_{k \in [T] \setminus \{i\}, d_{i,k} > D_{i,m}} \exp(\mathfrak{R}_{i,k,l} - \mathfrak{R}_{i,j,l})}{\sum_{k \in [T] \setminus \{i\}, d_{i,k} = D_{i,m}} \exp(\mathfrak{R}_{i,k,l} - \mathfrak{R}_{i,j,l})} \right). \end{aligned} \quad (12)$$

By plugging Eq. (10) and Eq. (11) into Eq. (12) we have

$$\mathcal{L}_{\text{VLO}} < \frac{1}{T(T-1)} \sum_{i=1}^T \sum_{m=1}^{M_i} n_{i,m} \log n_{i,m} + \epsilon = L^* + \epsilon \quad (13)$$

(3) We will show  $\forall 0 < \delta < 1$ , there is a

$$\epsilon = \frac{1}{T(T-1)} \min \left( \min_{i \in [T], m \in [M_i]} \log \left( 1 + \frac{1}{n_{i,m} \exp(\delta + \frac{1}{\delta})} \right), 2 \log \frac{1 + \exp(\delta)}{2} - \delta \right) > 0,$$

such that when  $\mathcal{L}_{\text{VLO}} < L^* + \epsilon$ , the representations satisfy VLO property. We first show that  $|\mathfrak{R}_{i,j,l} - \mathfrak{R}_{i,k,l}| < \delta$  if  $d_{i,j} = d_{i,k}$ ,  $i \in [T], j, k \in [T] \setminus \{i\}$  when  $\mathcal{L}_{\text{VLO}} < L^* + \epsilon$ . From Eq. (7) we have

$$\mathcal{L}_{\text{VLO}} > -\frac{1}{T(T-1)} \sum_{i=1}^T \sum_{m=1}^{M_i} \sum_{j \in [T] \setminus \{i\}, d_{i,j} = D_{i,m}} \log \frac{\exp(\mathfrak{R}_{i,j,l})}{\sum_{k \in [T] \setminus \{i\}, d_{i,k} = D_{i,m}} \exp(\mathfrak{R}_{i,k,l})} \quad (14)$$

Let  $p_{i,m} := \arg \min_{j \in [T] \setminus \{i\}, d_{i,j} = D_{i,m}} \mathfrak{R}_{i,j,l}$ ,  $q_{i,m} := \arg \max_{j \in [T] \setminus \{i\}, d_{i,j} = D_{i,m}} \mathfrak{R}_{i,j,l}$ ,  $\zeta_{i,m} := \mathfrak{R}_{i,p_{i,m},l}$ ,  $\eta_{i,m} := s_{i,q_{i,m},l} - s_{i,p_{i,m},l}$ ,  $\forall i \in [T]$ ,  $m \in [M_i]$ , by splitting out the maximum term and the minimum term we have

$$\begin{aligned} \mathcal{L}_{\text{VLO}} &> -\frac{1}{T(T-1)} \sum_{i=1}^T \sum_{m=1}^{M_i} \left\{ \log \frac{\exp(\zeta_{i,m})}{\sum_{k \in [T] \setminus \{i\}, d_{i,k} = D_{i,m}} \exp(\mathfrak{R}_{i,k,l})} \right. \\ &\quad \left. + \log \frac{\exp(\zeta_{i,m} + \eta_{i,m})}{\sum_{k \in [T] \setminus \{i\}, d_{i,k} = D_{i,m}} \exp(\mathfrak{R}_{i,k,l})} + \log \frac{\exp\left(\sum_{j \in [T] \setminus \{i, p_{i,m}, q_{i,m}\}, d_{i,j} = D_{i,m}} \mathfrak{R}_{i,j,l}\right)}{\left(\sum_{k \in [T] \setminus \{i\}, d_{i,k} = D_{i,m}} \exp(\mathfrak{R}_{i,k,l})\right)^{n_{i,m}-2}} \right\}. \end{aligned} \quad (15)$$

Let  $\theta_{i,m} := \frac{1}{n_{i,m}-2} \sum_{j \in [T] \setminus \{i, p_{i,m}, q_{i,m}\}, d_{i,j} = D_{i,m}} \exp(\mathfrak{R}_{i,j,l} - \zeta_{i,m})$ , we have

$$-\log \frac{\exp(\zeta_{i,m})}{\sum_{k \in [T] \setminus \{i\}, d_{i,k} = D_{i,m}} \exp(\mathfrak{R}_{i,k,l})} = \log(1 + \exp(\eta_{i,m}) + (n_{i,m} - 2)\theta_{i,m}) \quad (16)$$

and

$$-\log \frac{\exp(\zeta_{i,m} + \eta_{i,m})}{\sum_{k \in [T] \setminus \{i\}, d_{i,k} = D_{i,m}} \exp(\mathfrak{R}_{i,k,l})} = \log(1 + \exp(\eta_{i,m}) + (n_{i,m} - 2)\theta_{i,m}) - \eta_{i,m} \quad (17)$$

Then, from Jensen's inequality, we know

$$\exp\left(\sum_{j \in [T] \setminus \{i, p_{i,m}, q_{i,m}\}, d_{i,j} = D_{i,m}} \mathfrak{R}_{i,j,l}\right) \leq \left(\frac{1}{n_{i,m}-2} \sum_{j \in [T] \setminus \{i, p_{i,m}, q_{i,m}\}, d_{i,j} = D_{i,m}} \exp(\mathfrak{R}_{i,j,l})\right)^{n_{i,m}-2}, \quad (18)$$

thus

$$-\log \frac{\exp\left(\sum_{j \in [T] \setminus \{i, p_{i,m}, q_{i,m}\}, d_{i,j} = D_{i,m}} \mathfrak{R}_{i,j,l}\right)}{\left(\sum_{k \in [T] \setminus \{i\}, d_{i,k} = D_{i,m}} \exp(\mathfrak{R}_{i,k,l})\right)^{n_{i,m}-2}} \geq (n_{i,m} - 2) \log(1 + \exp(\eta_{i,m}) + (n_{i,m} - 2)\theta_{i,m}) - (n_{i,m} - 2) \log(\theta_{i,m}) \quad (19)$$

By plugging Eq. (16), Eq. (17) and Eq. (19) into Eq. (15), we have

$$\mathcal{L}_{\text{VLO}} > \frac{1}{T(T-1)} \sum_{i=1}^T \sum_{m=1}^{M_i} (n_{i,m} \log(1 + \exp(\eta_{i,m}) + (n_{i,m} - 2)\theta_{i,m}) - \eta_{i,m} - (n_{i,m} - 2) \log(\theta_{i,m})). \quad (20)$$

Let  $h(\theta) := n_{i,m} \log(1 + \exp(\eta_{i,m}) + (n_{i,m} - 2)\theta) - \eta_{i,m} - (n_{i,m} - 2) \log(\theta)$ . From derivative analysis we know  $h(\theta)$  decreases monotonically when  $\theta \in \left[1, \frac{1 + \exp(\eta_{i,m})}{2}\right]$  and increases monotonically when  $\theta \in \left[\frac{1 + \exp(\eta_{i,m})}{2}, \exp(\eta_{i,m})\right]$ , thus

$$h(\theta) \geq h\left(\frac{1 + \exp(\eta_{i,m})}{2}\right) = n_{i,m} \log n_{i,m} + 2 \log \frac{1 + \exp(\eta_{i,m})}{2} - \eta_{i,m}. \quad (21)$$

By plugging Eq. (21) into Eq. (20), we have

$$\begin{aligned}\mathcal{L}_{\text{VLO}} &> \frac{1}{T(T-1)} \sum_{i=1}^T \sum_{m=1}^{M_i} \left( n_{i,m} \log n_{i,m} + 2 \log \frac{1 + \exp(\eta_{i,m})}{2} - \eta_{i,m} \right) \\ &= L^* + \frac{1}{T(T-1)} \sum_{i=1}^T \sum_{m=1}^{M_i} \left( 2 \log \frac{1 + \exp(\eta_{i,m})}{2} - \eta_{i,m} \right)\end{aligned}\quad (22)$$

Then, since  $\eta_{i,m} \geq 0$ , we have  $2 \log \frac{1 + \exp(\eta_{i,m})}{2} - \eta_{i,m} \geq 0$ . Thus,  $\forall i \in [T], m \in [M_i]$ ,

$$\mathcal{L}_{\text{VLO}} > L^* + \frac{1}{T(T-1)} \left( 2 \log \frac{1 + \exp(\eta_{i,m})}{2} - \eta_{i,m} \right)\quad (23)$$

If  $\mathcal{L}_{\text{VLO}} < L^* + \epsilon \leq L^* + \frac{1}{T(T-1)} \left( 2 \log \frac{1 + \exp(\delta)}{2} - \delta \right)$ , then

$$2 \log \frac{1 + \exp(\eta_{i,m})}{2} - \eta_{i,m} < 2 \log \frac{1 + \exp(\delta)}{2} - \delta\quad (24)$$

Since  $y(x) = 2 \log \frac{1 + \exp(x)}{2} - x$  increases monotonically when  $x > 0$ , we have  $\eta_{i,m} < \delta$ . Hence  $\forall i \in [T], j, k \in [T] \setminus \{i\}$ , if  $d_{i,j} = d_{i,k} = D_{i,m}$ ,  $|\mathfrak{R}_{i,j,l} - \mathfrak{R}_{i,k,l}| \leq \eta_{i,m} < \delta$ . Next, we show  $\mathfrak{R}_{i,j,l} > \mathfrak{R}_{i,k,l} + \delta$  if  $d_{i,j} < d_{i,k}$  when  $\mathcal{L}_{\text{VLO}} < L^* + \epsilon$ . From Eq. (7) we have

$$\begin{aligned}\mathcal{L}_{\text{VLO}} &= -\frac{1}{T(T-1)} \sum_{i=1}^T \sum_{m=1}^{M_i} \sum_{j \in [T] \setminus \{i\}, d_{i,j} = D_{i,m}} \log \frac{\exp(\mathfrak{R}_{i,j,l})}{\sum_{k \in [T] \setminus \{i\}, d_{i,k} = D_{i,m}} \exp(\mathfrak{R}_{i,k,l})} \\ &\quad + \frac{1}{T(T-1)} \sum_{i=1}^T \sum_{m=1}^{M_i} \sum_{j \in [T] \setminus \{i\}, d_{i,j} = D_{i,m}} \log \left( 1 + \frac{\sum_{k \in [T] \setminus \{i\}, d_{i,k} = D_{i,m}} \exp(\mathfrak{R}_{i,k,l} - \mathfrak{R}_{i,j,l})}{\sum_{k \in [T] \setminus \{i\}, d_{i,k} > D_{i,m}} \exp(\mathfrak{R}_{i,k,l} - \mathfrak{R}_{i,j,l})} \right),\end{aligned}\quad (25)$$

and combining it with Eq. (8) we have

$$\begin{aligned}\mathcal{L}_{\text{VLO}} &\geq L^* + \frac{1}{T(T-1)} \sum_{i=1}^T \sum_{m=1}^{M_i} \sum_{j \in [T] \setminus \{i\}, d_{i,j} = D_{i,m}} \log \left( 1 + \frac{\sum_{k \in [T] \setminus \{i\}, d_{i,k} > D_{i,m}} \exp(\mathfrak{R}_{i,k,l} - \mathfrak{R}_{i,j,l})}{\sum_{k \in [T] \setminus \{i\}, d_{i,k} = D_{i,m}} \exp(\mathfrak{R}_{i,k,l} - \mathfrak{R}_{i,j,l})} \right) \\ &> L^* + \frac{1}{T(T-1)} \log \left( 1 + \frac{\exp(\mathfrak{R}_{i,k,l} - \mathfrak{R}_{i,j,l})}{\sum_{h \in [T] \setminus \{i\}, d_{i,h} = d_{i,j}} \exp(\mathfrak{R}_{i,h,l} - \mathfrak{R}_{i,j,l})} \right),\end{aligned}\quad (26)$$

$\forall i \in [T], j \in [T] \setminus \{i\}, k \in \{k \in [T] \setminus \{i\} \mid d_{i,j} < d_{i,k}\}$ . When  $\mathcal{L}_{\text{VLO}} < L^* + \epsilon$ , we already have  $|\mathfrak{R}_{i,h,l} - \mathfrak{R}_{i,j,l}| < \delta, \forall d_{i,h} = d_{i,j}$ , which derives  $\mathfrak{R}_{i,h,l} - \mathfrak{R}_{i,j,l} < \delta$  and thus  $\exp(\mathfrak{R}_{i,h,l} - \mathfrak{R}_{i,j,l}) < \exp(\delta)$ . By putting this into Eq. (25), we have  $\forall i \in [T], j \in [T] \setminus \{i\}, k \in \{k \in [T] \setminus \{i\} \mid d_{i,j} < d_{i,k}\}$ ,

$$\mathcal{L}_{\text{VLO}} > L^* + \frac{1}{T(T-1)} \log \left( 1 + \frac{\exp(\mathfrak{R}_{i,k,l} - \mathfrak{R}_{i,j,l})}{n_{i,r_{i,j}} \exp(\delta)} \right)\quad (27)$$

where  $r_{i,j} \in [M_i]$  is the index such that  $D_{i,r_{i,j}} = d_{i,j}$ .

Further, given  $\mathcal{L}_{\text{VLO}} < L^* + \epsilon < L^* + \frac{1}{T(T-1)} \log \left( 1 + \frac{1}{n_{i,r_{i,j}} \exp(\delta + \frac{1}{\delta})} \right)$ , we have

$$\log \left( 1 + \frac{\exp(\mathfrak{R}_{i,k,l} - \mathfrak{R}_{i,j,l})}{n_{i,r_{i,j}} \exp(\delta)} \right) < \log \left( 1 + \frac{1}{n_{i,r_{i,j}} \exp(\delta + \frac{1}{\delta})} \right) \quad (28)$$

which derives  $\mathfrak{R}_{i,j,l} > \mathfrak{R}_{i,k,l} + \frac{1}{\delta}, \forall i \in [T], j \in [T] \setminus \{i\}, k \in \{[T] \setminus \{i\} \mid d_{i,j} < d_{i,k}\}$ . Finally,  $\forall i \in [T], j, k \in [T] \setminus \{i\}, \mathfrak{R}_{i,j,l} < \mathfrak{R}_{i,k,l} - \frac{1}{\delta}$  if  $d_{i,j} > d_{i,k}$  directly follows from  $\mathfrak{R}_{i,j,l} > \mathfrak{R}_{i,k,l} + \frac{1}{\delta}$  if  $d_{i,j} < d_{i,k}$ .  $\square$

## A.2. Proofs of Theorem 4.3

**Setup and Assumptions.** To provide the vision-language continuity, we first assume that the frame embeddings  $\{\mathbf{v}_t\}$ , where  $t \in [1, T]$  are regularized under a Brownian Bridge process  $\mathbf{B}(t)$  as discussed in Section 4.2, where the transition density for any intermediate time  $t \in [n(i), n(j)]$  within a sampled interval is given as:

$$\mathbf{B}(t) \sim \mathcal{N}(\mathbb{E}[\mathbf{B}(t)], \text{Var}[\mathbf{B}(t)]), \quad (29)$$

with:

$$\mathbb{E}[\mathbf{B}(t)] = \mathbf{v}_i + \frac{t - n(i)}{n(j) - n(i)}(\mathbf{v}_j - \mathbf{v}_i), \quad \text{Var}[\mathbf{B}(t)] = \frac{(t - n(i))(n(j) - t)}{n(j) - n(i)}. \quad (30)$$

All time steps  $t \in [1, T]$  are covered by at least one sampled interval, ensuring the entire video sequence satisfies the Brownian Bridge regularization. Now, let  $\mathbf{v}_k, \mathbf{v}_l \in \mathbb{R}^d$  be arbitrary embeddings, *not necessarily* the endpoints  $\mathbf{v}_i$  and  $\mathbf{v}_j$  of a sampled interval. These embeddings fall within the *union*  $\mathfrak{U}$  of all sampled local intervals. Without loss of generality, here we can identify the interval  $[n(i), n(j)] \in \mathfrak{U}$  from the union containing  $\mathbf{v}_k$  and  $\mathbf{v}_l$ .

**Bounding Local Continuity.** Recall that semantic alignment score  $\mathfrak{R}(\mathbf{v}_k, \mathbf{v}_l, \mathbf{l})$  is defined as:

$$\mathfrak{R}(\mathbf{v}_k, \mathbf{v}_l, \mathbf{l}) = -\|\text{sim}(\mathbf{v}_k, \mathbf{l}) - \text{sim}(\mathbf{v}_l, \mathbf{l})\|_2,$$

where  $\text{sim}(\cdot)$  is Lipschitz continuous with constant  $C > 0$  when embeddings are normalized as unit vectors. By the Lipschitz continuity of  $\text{sim}(\cdot)$ , we have:

$$\|\text{sim}(\mathbf{v}_k, \mathbf{l}) - \text{sim}(\mathbf{v}_l, \mathbf{l})\|_2 \leq C \cdot \|\mathbf{v}_k - \mathbf{v}_l\|_2.$$

To ensure the continuity of  $\mathfrak{R}$ , we must bound  $\|\mathbf{v}_k - \mathbf{v}_l\|_2$ . Under the Brownian Bridge regularization, the embeddings are aligned with the mean trajectory  $\mathbb{E}[\mathbf{B}(t)]$ , and deviations are constrained by the variance  $\text{Var}[\mathbf{B}(t)]$ . Specifically:

$$\|\mathbf{v}_t - \mathbb{E}[\mathbf{B}(t)]\|_2^2 \leq \lambda \cdot \text{Var}[\mathbf{B}(t)],$$

where  $\lambda > 0$  depends on the strength of the Brownian Bridge loss  $\mathcal{L}_{\text{BB}}$ . Below we omit  $\lambda$  for simplicity. Substituting the variance:

$$\text{Var}[\mathbf{B}(t)] = \frac{(t - n(i))(n(j) - t)}{n(j) - n(i)}.$$

**Bounding Pairwise Distance.** The total pairwise distance between  $\mathbf{v}_k$  and  $\mathbf{v}_l$  can be expressed as:

$$\|\mathbf{v}_k - \mathbf{v}_l\|_2 \leq \|\mathbb{E}[\mathbf{B}(k)] - \mathbb{E}[\mathbf{B}(l)]\|_2 + \sqrt{\text{Var}[\mathbf{B}(k)]} + \sqrt{\text{Var}[\mathbf{B}(l)]}.$$

Since the mean trajectory  $\mathbb{E}[\mathbf{B}(t)]$  is linear within the interval  $[n(i), n(j)]$ , we have:

$$\|\mathbb{E}[\mathbf{B}(k)] - \mathbb{E}[\mathbf{B}(l)]\|_2 \leq \frac{|k - l|}{n(j) - n(i)} \|\mathbf{v}_j - \mathbf{v}_i\|_2.$$

Combining these bounds, now we can rewrite into the following inequality:

$$\|\mathbf{v}_k - \mathbf{v}_l\|_2 \leq \frac{|k - l|}{n(j) - n(i)} \|\mathbf{v}_j - \mathbf{v}_i\|_2 + \sqrt{\frac{(k - n(i))(n(j) - k)}{n(j) - n(i)}} + \sqrt{\frac{(l - n(i))(n(j) - l)}{n(j) - n(i)}}.$$



For the variance terms, the Brownian Bridge process achieves its maximum variance at the midpoint  $t = \frac{n(i)+n(j)}{2}$ . This gives us,

$$\text{Var}[\mathbf{B}(t_{\max})] = \frac{n(j) - n(i)}{4}, \quad \|\mathbf{v}_k - \mathbf{v}_l\|_2 \leq 2 \frac{|k-l|}{n(j) - n(i)} + \sqrt{(n(j) - n(i))}.$$

**Bounding Semantic Alignment Score.** Finally, by substituting this bound into the Lipschitz continuity of  $\text{sim}$ , we obtain,

$$|\mathfrak{R}(\mathbf{v}_k, \mathbf{v}_l, \mathbf{l})| \leq C \cdot \left( \frac{2|k-l|}{n(j) - n(i)} + \sqrt{(n(j) - n(i))} \right).$$

To ensure  $|\mathfrak{R}(\mathbf{v}_k, \mathbf{v}_l, \mathbf{l})| < \epsilon$ , we require:

$$C \cdot \left( 2 \frac{|k-l|}{n(j) - n(i)} + \sqrt{n(j) - n(i)} \right) < \epsilon.$$

Here, we consider these two terms respectively:

$$2C \frac{|k-l|}{n(j) - n(i)} < \frac{\epsilon}{2}, \quad C \sqrt{n(j) - n(i)} < \frac{\epsilon}{2},$$

which gives:

$$|k-l| < \delta_1 = \frac{\epsilon \cdot (n(j) - n(i))}{4C}, \quad n(j) - n(i) < \left( \frac{\epsilon}{2C} \right)^2.$$

Combining these conditions, we choose:

$$\delta = \min \left( \frac{\epsilon \cdot (n(j) - n(i))}{4C}, \frac{\epsilon^2}{4C^2} \right).$$

**Final Conclusion.** For any given  $\epsilon > 0$ , setting  $\delta = \min \left( \frac{\epsilon \cdot (n(j) - n(i))}{4C}, \frac{\epsilon^2}{4C^2} \right)$  ensures:

$$\|\mathbf{v}_k - \mathbf{v}_l\|_2 < \delta \quad \Rightarrow \quad |\mathfrak{R}(\mathbf{v}_k, \mathbf{v}_l, \mathbf{l})| < \epsilon.$$

□

### A.3. Proof of Theorem 4.4

From the definition of the semantic alignment score, we have:

$$\mathfrak{R}(\mathbf{v}_i, \mathbf{v}_j, \mathbf{l}) = -|\text{sim}(\mathbf{v}_i, \mathbf{l}) - \text{sim}(\mathbf{v}_j, \mathbf{l})|, \quad \mathfrak{R}(\mathbf{v}_i, \mathbf{v}_j, \mathbf{l}') = -|\text{sim}(\mathbf{v}_i, \mathbf{l}') - \text{sim}(\mathbf{v}_j, \mathbf{l}')|.$$

The difference in scores can be bounded using the reverse triangle inequality:

$$|\mathfrak{R}(\mathbf{v}_i, \mathbf{v}_j, \mathbf{l}') - \mathfrak{R}(\mathbf{v}_i, \mathbf{v}_j, \mathbf{l})| \leq |(\text{sim}(\mathbf{v}_i, \mathbf{l}') - \text{sim}(\mathbf{v}_j, \mathbf{l}')) - (\text{sim}(\mathbf{v}_i, \mathbf{l}) - \text{sim}(\mathbf{v}_j, \mathbf{l}))|.$$

Simplifying the inequalities above, it gives us:

$$|\mathfrak{R}(\mathbf{v}_i, \mathbf{v}_j, \mathbf{l}') - \mathfrak{R}(\mathbf{v}_i, \mathbf{v}_j, \mathbf{l})| \leq |\text{sim}(\mathbf{v}_i, \mathbf{l}') - \text{sim}(\mathbf{v}_i, \mathbf{l})| + |\text{sim}(\mathbf{v}_j, \mathbf{l}') - \text{sim}(\mathbf{v}_j, \mathbf{l})|.$$

By the Lipschitz continuity of  $\text{sim}$ , we have: for some constant  $C > 0$ ,

$$|\text{sim}(\mathbf{v}_i, \mathbf{l}') - \text{sim}(\mathbf{v}_i, \mathbf{l})| \leq C \|\mathbf{l}' - \mathbf{l}\|_2, \quad |\text{sim}(\mathbf{v}_j, \mathbf{l}') - \text{sim}(\mathbf{v}_j, \mathbf{l})| \leq C \|\mathbf{l}' - \mathbf{l}\|_2.$$

Substituting these bounds and considering  $\|\mathbf{l}' - \mathbf{l}\|_2 \leq \delta_l$

$$|\mathfrak{R}(\mathbf{v}_i, \mathbf{v}_j, \mathbf{l}') - \mathfrak{R}(\mathbf{v}_i, \mathbf{v}_j, \mathbf{l})| \leq 2C \|\mathbf{l}' - \mathbf{l}\|_2 \leq 2C \delta_l. \quad (31)$$

□

## B. Pre-training Details

Following (Ma et al., 2023a; Li et al., 2024), we use a modified ResNet-50 (He et al., 2016) from CLIP (Radford et al., 2021) for the vision encoder and a CLIP transformer for the language encoder. We initialize our model with CLIP and train them on EPIC-KITCHEN-100 (Damen et al., 2018; 2020). The training hyperparameters used during the pre-training are listed in Table 3. For  $\mathcal{L}_{BB}$ , due to the large number of video frames, we apply a logarithmic scaling to the variance term. The training was conducted on two NVIDIA A800 GPUs, and the process took approximately 30 hours.

Table 3. Hyper-parameters for pre-training.

| Config                   | value                   |
|--------------------------|-------------------------|
| Training epochs          | 1000                    |
| Optimizer                | Adam                    |
| Learning rate            | $1 \times 10^{-5}$      |
| Batch size               | 128                     |
| Sampled frames per video | 10                      |
| Weight decay             | 0.001                   |
| Optimizer momentum       | 0.9, 0.999              |
| Data augmentation        | <i>RandomCropResize</i> |

## C. Evaluation Details

### C.1. Simulation Environments

We follow (Nair et al., 2022) for the specific simulation environment setup and code details.

**Franka Kitchen.** The Franka Kitchen environment (Gupta et al., 2019; Fu et al., 2020) is based on the 9 degrees of freedom Franka robot. The Franka robot is placed in a kitchen environment containing several common household items: a microwave, a kettle, an overhead light, cabinets, and an oven. Following (Nair et al., 2022), the Franka Kitchen environments used in this paper are modified from their original design. Specifically, we introduce additional randomization to the scene by randomly altering the kitchen’s position between episodes. This modification makes the tasks significantly more challenging in terms of both perception and control.

**Metaworld.** The Metaworld environment (Yu et al., 2019) is an open-source simulated benchmark for robot learning. In our settings, the target object position is randomized between episodes in all tasks.

We present the specific language instructions for each tasks in Table 4.

Table 4. Language Instructions for tasks in Franka Kitchen and Metaworld.

| Environment ID                          | Language Instruction                  |
|---|---------------------------------------|
| kitchen_micro_open-v3                   | open microwave                        |
| kitchen_sdoor_open-v3                   | slide cabinet                         |
| kitchen_ldoor_open-v3                   | open left door                        |
| kitchen_knob1_on-v3                     | turn on stove                         |
| kitchen_light_on-v3                     | switch on light                       |
| hammer-v2-goal-observable               | hammer nail                           |
| button-press-topdown-v2-goal-observable | press button                          |
| bin-picking-v2-goal-observable          | pick and place the block between bins |
| assembly-v2-goal-observable             | assemble the ring onto peg            |

### C.2. Language-Conditioned Behavior Cloning Hyperparameters

We present the LCBC imitation learning hyperparameters in Table 5. For each distinct evaluation task, we perform policy evaluation every 1,000 gradient steps by running 50 rollouts and computing their average success rate. Over a total of 10,000 gradient steps, we conduct this evaluation 10 times. The highest success rate among these 10 evaluations is reported as the final result. To ensure robustness, we average the results across two different camera viewpoints and three independent random seeds.

Table 5. Hyper-parameters for LCBC.

|                       | Franka Kitchen     | Metaworld          |
|-----------------------|--------------------|--------------------|
| MLP achitecture       | [256,256]          | [256,256]          |
| Non-linear activation | ReLU               | ReLU               |
| Optimizer             | Adam               | Adam               |
| Gradient Steps        | 10K                | 10K                |
| Learning rate         | $1 \times 10^{-3}$ | $1 \times 10^{-3}$ |
| Batch size            | 32                 | 32                 |
| Horizon               | 50                 | 100                |
| Proprioception        | 9                  | 4                  |

### C.3. Language-Conditioned Behavior Cloning Results

In Table 6- 11, we report detailed Language-Conditioned Behavior Cloning results for different task and dataset size. The results demonstrate that our method achieves significant improvements across different simulation environments, varying dataset sizes, and diverse robotic manipulation tasks.

Table 6. LCBC results when dataset size= 5 on Franka Kitchen.

| Method       | Slide Cabinet | Open Left Door | Open Microwave | Turn On Stove | Switch On Light | Average     |
|--------------|---------------|----------------|----------------|---------------|-----------------|-------------|
| CLIP         | 38.7          | 2.0            | 3.0            | 7.0           | 7.7             | 11.7        |
| R3M          | 68.7          | 18.3           | 7.7            | 19.3          | 29.0            | 28.6        |
| LIV          | 55.0          | 6.0            | 7.0            | 13.0          | 22.0            | 20.6        |
| DecisionNCE  | 59.3          | 9.7            | 7.0            | <b>26.3</b>   | 24.3            | 25.3        |
| AcTOL w/o BB | 71.5          | 11.5           | 10.5           | 23.5          | 47.0            | 32.8        |
| AcTOL        | <b>85.5</b>   | <b>20.0</b>    | <b>18.3</b>    | 24.7          | <b>62.3</b>     | <b>42.6</b> |

### C.4. Language-Conditioned Visual Reward Results

As shown in Figure 6, we present more visualizations of Language-Conditioned Visual Reward on real-world robot manipulation videos from (Bahl et al., 2022). In Figure 6(a), the robot performs two consecutive and opposing actions. Our method effectively identifies the action boundaries and generates the correct reward sequence, increasing first and then decreasing, in alignment with the given instructions. In Figures 6(b)-(d), where the robot performs a single action, the robot initially moves slowly as it searches for the target. Correspondingly, the reward grows gradually. Once the robot interacts with the object and completes the task, our method captures the distinct semantic changes in the action, leading to a rapid reward increase. In Figures 6(e)-(f), we test two complex actions and instructions to explore the limits of our method. In Figure 6(e), the model is required to accurately distinguish between the blue and red cups to complete the task. In Figure 6(f), the model needs to differentiate the orientation and face values of two dice. These scenarios impose high demands on the model’s visual and semantic understanding. Our method successfully produces the correct rewards in both tasks, showcasing its potential for application in real-world, complex scenarios.

Table 7. LCBC results when dataset size= 15 on Franka Kitchen.

| Method       | Slide Cabinet | Open Left Door | Open Microwave | Turn On Stove | Switch On Light | Average     |
|--------------|---------------|----------------|----------------|---------------|-----------------|-------------|
| CLIP         | 71.0          | 8.0            | 15.7           | 14.7          | 28.0            | 27.5        |
| R3M          | 81.0          | 31.0           | 22.0           | 19.3          | 57.7            | 42.2        |
| LIV          | 85.0          | 19.0           | 28.3           | 29.7          | 51.7            | 42.7        |
| DecisionNCE  | 92.0          | 18.7           | 27.0           | 33.3          | 45.0            | 43.2        |
| AcTOL w/o BB | 84.5          | 29.5           | 29.5           | <b>54.0</b>   | 73.5            | 54.2        |
| AcTOL        | <b>99.5</b>   | <b>37.5</b>    | <b>37.0</b>    | 53.5          | <b>81.5</b>     | <b>61.8</b> |

Table 8. LCBC results when dataset size= 25 on Franka Kitchen.

| Method       | Slide Cabinet | Open Left Door | Open Microwave | Turn On Stove | Switch On Light | Average     |
|--------------|---------------|----------------|----------------|---------------|-----------------|-------------|
| CLIP         | 66.3          | 8.7            | 18.7           | 23.7          | 38.7            | 31.2        |
| R3M          | 84.7          | 35.3           | 40.0           | 34.0          | 61.7            | 51.1        |
| LIV          | 91.7          | 26.0           | 35.0           | 45.3          | 61.7            | 51.9        |
| DecisionNCE  | 91.7          | 27.0           | 37.0           | 47.3          | 51.3            | 50.9        |
| AcTOL w/o BB | 92.0          | <b>37.0</b>    | 40.0           | 57.0          | 78.0            | 60.8        |
| AcTOL        | <b>100.0</b>  | <b>37.0</b>    | <b>42.5</b>    | <b>62.5</b>   | <b>81.0</b>     | <b>64.6</b> |

Table 9. LCBC results when dataset size= 5 on Metaworld.

| Method       | Assembly    | Pick bin    | Press button | Hammer      | Average     |
|--------------|-------------|-------------|--------------|-------------|-------------|
| CLIP         | 48.3        | 35.3        | 34.3         | 51.2        | 42.3        |
| R3M          | 63.5        | 33.3        | 27.3         | 63.2        | 46.8        |
| LIV          | 61.8        | 32.3        | 32.7         | 61.0        | 47.0        |
| DecisionNCE  | 54.0        | 31.0        | 27.7         | 65.7        | 44.6        |
| AcTOL w/o BB | <b>66.8</b> | 39.0        | 20.7         | <b>74.7</b> | 50.3        |
| AcTOL        | 62.8        | <b>41.0</b> | <b>42.0</b>  | 69.5        | <b>53.8</b> |

Table 10. LCBC results when dataset size= 15 on Metaworld.

| Method       | Assembly    | Pick bin    | Press button | Hammer      | Average     |
|--------------|-------------|-------------|--------------|-------------|-------------|
| CLIP         | 73.0        | 40.3        | 52.0         | 76.0        | 60.3        |
| R3M          | 80.7        | 17.0        | 45.0         | 83.3        | 56.5        |
| LIV          | 84.3        | 37.0        | 54.7         | 81.3        | 64.3        |
| DecisionNCE  | 73.3        | 36.7        | 43.3         | 83.0        | 59.1        |
| AcTOL w/o BB | <b>94.0</b> | 50.3        | 48.3         | <b>90.7</b> | 70.8        |
| AcTOL        | 82.5        | <b>64.5</b> | <b>65.5</b>  | 84.0        | <b>74.1</b> |

Table 11. LCBC results when dataset size= 25 on Metaworld.

| Method       | Assembly    | Pick bin    | Press button | Hammer      | Average     |
|--------------|-------------|-------------|--------------|-------------|-------------|
| CLIP         | 69.3        | 36.0        | 66.0         | 78.8        | 62.5        |
| R3M          | 87.7        | 14.7        | 48.3         | 89.7        | 60.1        |
| LIV          | 87.3        | 23.7        | 66.0         | 89.7        | 66.7        |
| DecisionNCE  | 85.7        | 47.0        | 58.0         | 88.3        | 69.8        |
| AcTOL w/o BB | <b>93.7</b> | 51.7        | 55.0         | <b>93.0</b> | 73.3        |
| AcTOL        | 93.5        | <b>66.0</b> | <b>76.5</b>  | 88.5        | <b>81.1</b> |



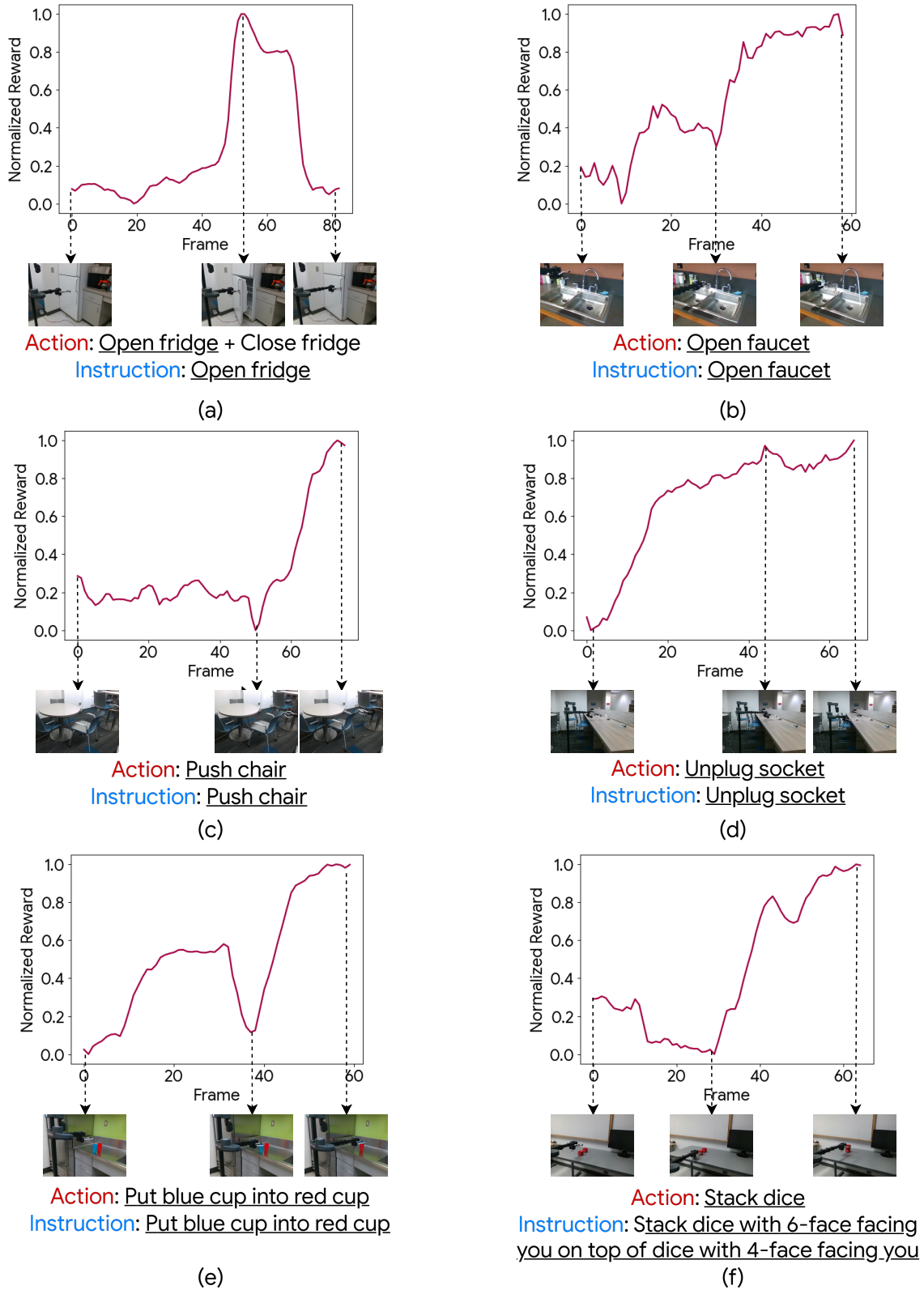


Figure 6. Reward plots for exemplar robot action videos.